



ISSN (O): 2320-5407  
ISSN (P): 3107-4928

Journal Homepage: [-www.journalijar.com](http://www.journalijar.com)

## INTERNATIONAL JOURNAL OF ADVANCED RESEARCH (IJAR)

Article DOI:10.21474/IJAR01/23541  
DOI URL: <http://dx.doi.org/10.21474/IJAR01/23541>



INTERNATIONAL JOURNAL OF  
ADVANCED RESEARCH (IJAR)  
ISSN 2320-5407  
Journal homepage: <http://www.journalijar.com>  
Journal DOI:10.21474/IJAR01

### RESEARCH ARTICLE

## SYNTHESIS AND CHARACTERIZATION OF ZEOLITIC CATALYSTS BY THE PLACKETT AND BURMAN (PB) PLAN METHOD USING LOCAL MATERIALS FROM NIGER

Adamou Ibro Abdourahamane<sup>1</sup>, IbrahLandiAli<sup>2</sup>, Amadou Kiari Mahamane Nassirou<sup>1</sup>, Manzola Abdou Salam<sup>3</sup>, Yao Kouassi Benjamin<sup>1</sup> and Soro Yaya<sup>1</sup>

1. Laboratoire des Procédés Industriels de Synthèse, de l'Environnement et des Energies Nouvelles (LAPISEN), Institut National Polytechnique Felix Houphouët Boigny (INP-HB) -Ecole Doctorale Polytechnique (EDP), Yamoussoukro-BP : 1093, Côte D'Ivoire.
2. Departement de chimie, Faculté des Sciences et Technique, Université Dan DickoDankoulodo (UDDM), Maradi, République du Niger.
3. Laboratoire Matériaux, Eaux et Environnement (LAMEE), Université Abdou Moumouni (UAM)- Faculté des Sciences et Techniques (FAST), Niamey-BP :10896/237, Niger.

#### Manuscript Info

##### Manuscript History

Received: 14 March 2026  
Final Accepted: 16 April 2026  
Published: May 2026

##### Key words:-

Clay, catalysts, cracking, naphtha, sand.

#### Abstract

Zeolite catalysts have become the most widely used materials in the crude oil refining industry. Zeolite catalysts were synthesized using clays (raw  $D_1$  and treated  $D_2$ ) and sand ( $S_M$ ) sampled in Niger (Maradi). Characterization tests were performed on  $D_1$ ,  $D_2$ , and  $S_M$  using conventional techniques (CEC, PAF, XRD, XRF, FT-IR, BET, and SEM). These techniques revealed the presence of 96% non-swelling clays and 4% swelling clays. The silica-alumina ratio (SAR) of the sand is 43.28. Based on these compositions, various chemical mixtures ( $D_1$ ,  $D_2$ ,  $S_M$ , aluminum isopropoxide  $Al(OCH(CH_3)_2)_3$  or  $Al(O-i-Pr)_3$ , sodium hydroxide NaOH, and distilled water) were prepared to synthesize the catalysts following the factor screening plan according to the Hadamard matrix. After synthesis, the experimental results showed that the influential factors are aluminum isopropoxide, clay, stirring time, drying time, and calcination temperature. Using the Boehm test, the screening plan made it possible to record a response characterizing the catalytic activity, namely the acidity ( $Y_{exp}$ ) on the surface of the catalysts. The results indicated that  $Y_{exp}$  of the catalysts varies between 15 and 65 meq/g. Three best catalysts, namely CAZ-1, 2, and 7, were selected based on  $Y_{exp}$  and then characterized (XRD, XRF, FT-IR, BET, SEM, and DTA-TGA).

"© 2026 by the Author(s). Published by IJAR under CC BY 4.0. Unrestricted use allowed with credit to the author."

**Corresponding Author:-**Adamou Ibro Abdourahamane

**Address:-**1. Laboratoire des Procédés Industriels de Synthèse, de l'Environnement et des Energies Nouvelles (LAPISEN), Institut National Polytechnique Felix Houphouët Boigny (INP-HB) -Ecole Doctorale Polytechnique (EDP), Yamoussoukro-BP : 1093, Côte D'Ivoire.

The results of the analyses carried out on the synthesized zeolite catalysts CAZ-1, CAZ-2, and CAZ-7 show that they have mineralogical, chemical, physical, morphological, and thermal characteristics similar to those of Y zeolite and intermediate Y zeolite zeolite catalysts. Of the three selected catalysts, CAZ-2 showed the best results, with a 10.85% increase in light molecules and a catalytic yield of 83%.

### Introduction:-

Over the years, zeolite catalysts with MFI (ZSM-5), Faujasite (X,YFAU), Beta zeolite (BEA), etc. structures have become the most widely used catalytic materials in the crude oil refining industry due to their high acidity and good shape selectivity(Armor, 2011; Degnan et al., 2000; Margeta & Farkaš, 2020; Zimmermann & Haranczyk, 2016). These catalysts can be synthesized from industrial materials such as Tetrapropyl ammonium (TPA), industrial silica (LUDOX HS-40), and Aluminum Isopropoxide (IP). The latter act respectively as a synthesis matrix or support, an additive providing hardness to the catalysts, and an additive providing the catalysts with reaction sites (Biligtu et al., 2017). Given not only the toxic and polluting nature of the industrial materials (TPA, LUDOX-HS40, IP, etc.) used during catalyst synthesis, but also their high cost, researchers have turned to a much more economical and environmentally friendly alternative using natural, accessible, and less expensive materials such as clay minerals(Yue et al., 2018). This led researchers such as Pan. F et al., 2017(Pan et al., 2017); Xing. Y et al., 2017 (Li et al., 2017); Nanzhe et al., 2019 (Liu et al., 2019); Yue. Y et al., 2020 (Yue et al., 2020), and Wu. M et al., 2020(Wu et al., 2020) have used kaolinite, attapulgite, illite, rectorite, and palygorskite, respectively, to synthesize zeolite catalysts. These catalysts are generally synthesized using two methods: the dry method, without solvents, in the experimental protocol, and the hydrothermal method (Liu et al., 2019; Pan et al., 2017; L. Zhang et al., 2018).The hydrothermal method remains the most suitable for synthesizing zeolite catalysts, as the solvent is necessary for proper crystallization of the catalysts(Wu et al., 2020).

The present work aims to synthesize zeolite catalysts by the hydrothermal process, using clay and sand sampled in Niger. Specifically, clay is used as a synthesis support and sand as a siliceous additive to replace certain industrial siliceous materials such as LUDOX HS-40 used by I. Qoniah et al., 2015(Qoniah et al., 2015) or Florisil used by O. Abdoulaye Dan Makaou et al., 2021(Abdoulaye Dan Makaou et al., 2021) in the synthesis of zeolite catalysts. To date, very little literature has been reported on work aimed at replacing industrial siliceous materials with natural sand in the synthesis of zeolite catalysts using the factor screening method according to the Hadamard matrix. This work aims to contribute further to this field.

After synthesizing zeolite catalysts using the factor screening method, they will be characterized using X-ray Diffraction (XRD), X-ray Fluorescence (XRF), Fourier Transform Infrared Spectroscopy (FT-IR), Brunauer-Emmett-Teller(BET), Scanning Electron Microscopy(SEM), and Thermogravimetric Analysis (TGA) and Differential Thermal Analysis (DTA)methods. These analytical methods will enable the structure of the synthesized catalysts, their chemical composition, chemical functions, textural properties, morphology, and mass variation as a function of temperature to be studied. Catalytic cracking tests were conducted on naphtha using the three (3) catalysts to determine their performance.

### Experimental:-

#### Materials:-

The clay used as a matrix in the catalyst synthesis procedure is a Nigerien kaolinite clay ( $D_1$  : raw clay and  $D_2$  : activated clay) which has been the subject of publication in previous work(Abdourahmane et al., 2022). It comprises 81.8% kaolinite, 14.2% illite and 4% smectite, i.e. 96% non-swelling clays (kaolinite and illite) and 4% swelling clays (smectite). Clay  $D_1$  has a BET specific surface area ( $S_S$ ) of 446.50 m<sup>2</sup>/g, a pore diameter (DP) of 2.12 nm and a micropore volume ( $V_{MP}$ ) of 0.22 cm<sup>3</sup>/g, while sample  $D_2$  has a BET specific surface area ( $S_S$ ) of 256.3 m<sup>2</sup>/g, a pore diameter (DP) of 2.10 nm and a micropore volume ( $V_{MP}$ ) of 0.12 cm<sup>3</sup>/g. The sand ( $S_M$ ) contains 94.78% SiO<sub>2</sub> and 1.90% Al<sub>2</sub>O<sub>3</sub>, giving a Silica Alumina Ratio (SAR) of 43.28. In addition to clay and sand, industrial chemicals were also used in the zeolite catalyst synthesis protocol: aluminum isopropoxide C<sub>9</sub>H<sub>21</sub>AlO<sub>3</sub> (Sigma-Aldrich, Lot#MKCM4214, Code=102340685, purity ≥ 98%), sodium hydroxide NaOH (Fisher-Chemical, Lot1870577, Code=S/4920/60, purity=98.99%) and distilled water.

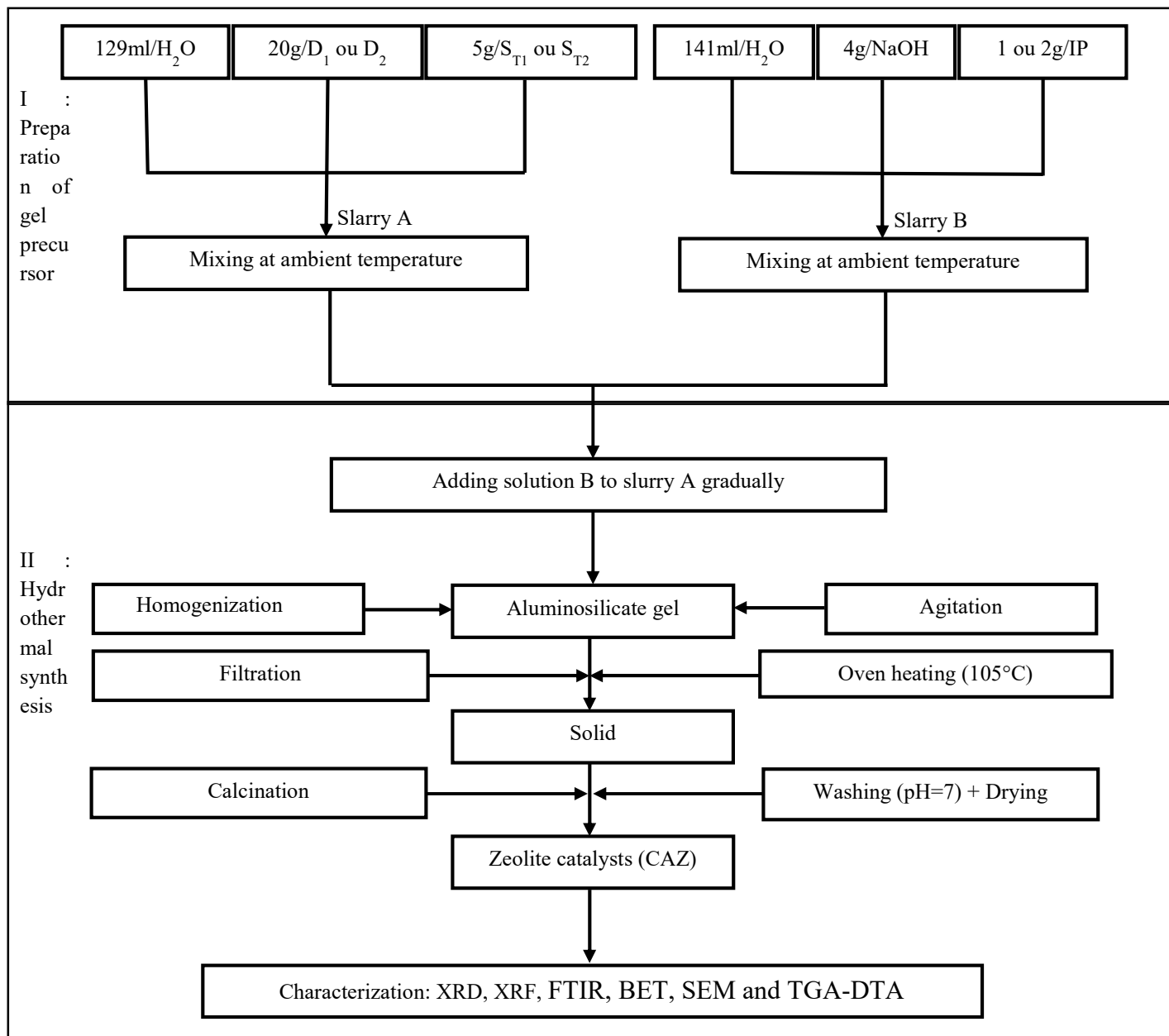
#### Catalyst synthesis:-

##### Synthesis protocol:-

Mixtures were prepared from clays ( $D_1$  or  $D_2$ ), sand ( $S_M$ ), sodium hydroxide, aluminum isopropoxide and water. The zeolite catalyst synthesis protocol, illustrated schematically in Fig.1., was inspired by the protocol of Reza Khoshbin

and al, 2017(Khoshbin& Karimzadeh, 2017). This protocol consists of four parts, but for ease of use, we have modified it into two parts, I and II (See Fig.1).In addition to this modification, we applied a design of experiments methodology to this protocol. This is the Plackett and Burman (PB) design.

Fig.1. Schematic flow chart for preparation steps of catalysts.



#### Synthesis optimization:-

Optimization was performed using experimental designs. The design used was that of Plackett and Burman (PB). This is a screening design based on a first-order response surface model, for k factors (quantitative or qualitative) at two levels +1 and -1, in which interactions are not taken into account. The model equation is as follows (*Plans d'expérience*, 2010):

$$y_N = b_0 + \sum_{i=1}^k b_i X_i(1)$$

With the number N of trials (here a multiple of 4,  $N = k+1$ ),  $b_0$  is the mean,  $b_i$  the effect of factors  $X_i$  and  $y_N$  the result of the experiment.

Table 1 below gives the characteristics and experimental ranges of the variable factors used for catalyst synthesis. In order to obtain catalysts with good catalytic characteristics, seven (7) factors were used: aluminum isopropoxide ( $X_1$ ), clay ( $X_2$ ), sand ( $X_3$ ), stirring time ( $X_4$ ), drying time ( $X_5$ ), calcination temperature ( $X_6$ ) and calcination time ( $X_7$ ). These factors were chosen, on the one hand, on the basis of the results of preliminary analyses of clays ( $D_1$  and  $D_2$ ) and sand ( $S_M$ ) and, on the other hand, on the basis of literature data.

**Table.1 Experimental domain.**

Factors	Symbol	-1	+1
Aluminum Isopropoxide (IP)	$X_1$	1g	2g
Clay (D)	$X_2$	Rawclay ( $D_1$ )	Activatedclay ( $D_2$ )
Sand ( $S_M$ )	$X_3$	18 $\mu\text{m}$ ( $S_{M1}$ )	24 $\mu\text{m}$ ( $S_{M2}$ )
Agitation Time (TA)	$X_4$	6h	10h
Drying Time (TS)	$X_5$	12h	24h
Calcination temperature ( $T^\circ\text{C}$ )	$X_6$	550 $^\circ\text{C}$	650 $^\circ\text{C}$
Calcination Time (TC)	$X_7$	3h	4h

Next, eight (8) trials were carried out, based on the construction principle of Hadamard's experiment matrix (Table 2) (Goupy & Creighton, 2006). This matrix is constructed from the sequence of + and - signs corresponding to the +1 and -1 level of the first row (*Plans d'expérience*, 2010). Hadamard's design is often used first to screen factors in order to obtain an initial assessment of their influence on the desired response, based on a reduced number of tests to be carried out in the Lab.

**Table2. Hadamard matrix.**

N° Exp	Coded values						
	$X_1$	$X_2$	$X_3$	$X_4$	$X_5$	$X_6$	$X_7$
1	+1	-1	+1	+1	-1	-1	+1
2	+1	+1	-1	+1	+1	-1	-1
3	-1	+1	+1	-1	+1	+1	-1
4	-1	-1	+1	+1	-1	+1	+1
5	+1	-1	-1	+1	+1	-1	+1
6	+1	+1	-1	-1	+1	+1	-1
7	-1	+1	+1	-1	-1	+1	+1
8	-1	-1	-1	-1	-1	-1	-1

After replacing the coded values with real values, the following Table 3 shows the experimental design.

**Table.3 Experimentation plan.**

CAZ	IP(g)	D (g)	$S_M$ ( $\mu\text{m}$ )	TA (h)	TS (h)	( $T^\circ\text{C}$ )	TC (h)
1	2	$D_1$	$S_{M2}$	10	12	550	4
2	2	$D_2$	$S_{M1}$	10	24	550	3
3	1	$D_2$	$S_{M2}$	6	24	650	3
4	1	$D_1$	$S_{M2}$	10	12	650	4
5	2	$D_1$	$S_{M1}$	10	24	550	4
6	2	$D_2$	$S_{M1}$	6	24	650	3
7	1	$D_2$	$S_{M2}$	6	12	650	4
8	1	$D_1$	$S_{M1}$	6	12	550	3

The synthesis technique involved first preparing a gel precursor by mixing two solutions A (slurry) and B (Part-I/ Fig.1). Slurry A is a mixture of 20g clays ( $D_1$  or  $D_2$ ),  $S_M$  Sand ( $S_{M1} = 18 \mu\text{m}$  or  $S_{M2} = 24 \mu\text{m}$ ) and distilled water (129 ml). Slurry B is a mixture of 4g NaOH, 1 or 2g aluminum isopropoxide and 141 mL distilled water. Next, hydrothermal synthesis (Part-II/ Fig.1) began after mixing solutions A and B. This mixture yielded an aluminosilicate gel. The latter was homogenized and stirred for 6 to 10 hours before being filtered and dried at

105°C for 12 to 24 hours in an oven, resulting in a solid. This was calcined at 550 or 650°C for 3 to 4 hours. Any carbonization residues were removed by thorough washing with distilled water until a pH close to neutrality was obtained. The resulting materials were cooled, dried and ground to a particle size ( $\phi$ ) of 18  $\mu\text{m}$ . These materials constitute our zeolite catalysts. The completion of these eight (8) experiments resulted in eight (8) corresponding zeolite catalysts. Zeolite catalysts are characterized by their activity, which is essentially related to surface acidity (Rabo & Gajda, 1990). A surface acidity or Surface Function (SF) test was carried out on the catalysts. The result of this test is called the  $Y_{\text{exp}}$  response.

Determination and quantification of catalyst surface functions was carried out using the BOEHM titration method (Contescu et al., 1997). This method enables functional groups with a range of acidities or basicities to be assayed with bases or acids respectively. The protocol used was as follows: a mass of 0.5 g of CAZs was brought into contact for 72 h, with stirring, in a 100 mL beaker, with 25 mL each of 0.1 N aqueous solutions of NaOH,  $\text{NaHCO}_3$ ,  $\text{Na}_2\text{CO}_3$  (determination of acid groups) and HCl (determination of basic groups) to ensure that as many of the catalyst surface groups as possible were reacted, then the mixture was filtered through What man paper (0.45 micron).

After filtration, titration of excess solutions was carried out using 0.1 N sodium hydroxide and hydrochloric acid solutions for the basic and acid functions respectively. The basic solutions were titrated with 0.1 N hydrochloric acid (HCl), using three (3) drops each of phenolphthalein, helianthin and bromothymol blue, and the acid solution with 0.1 N sodium hydroxide (NaOH), with phenolphthalein as the color indicator. Since this is a back assay, the number of moles of the desired function is equivalent to the number of moles reacted with the contact solution. Quantification of acidic and basic groups is performed using the following formula:

$$\text{Surfacefunction} \left( \frac{\text{meq}}{\text{g}} \right) = \frac{n_{\text{react}}}{m_{\text{CAZ}}} * 100 \quad (2)$$

#### Where

n (reacts) : quantity of material (acid or base) reacted (meq);

m (CAZ) : mass of catalyst (g).

The results obtained were processed using Nemrod software (version 9901 French, LPRAI-Marseille Inc., France) for factor screening. The factor significance test was performed by calculating the experimental error (Equations (3) and (4)).

$$\sigma_e = \frac{\sigma}{\sqrt{N}} \quad (3) \quad \text{and} \quad \sigma = \sqrt{\frac{1}{N-p} \sum_1^N (Y_i - \hat{Y}_i)^2} \quad (4)$$

#### Where

$\sigma_e$  is the experimental error,  $\sigma$  is the standard deviation, N is the number of repetitions, p is the number of coefficients,  $Y_i$  is the experimental response and  $\hat{Y}_i$  is the response predicted by the model.

The following equation (5) was used to calculate the contribution of each factor to the acidity of the synthesized zeolite catalysts (Goupy & Creighton, 2006).

$$P_i = \left( \frac{b_i^2}{\sum b_i^2} \right) * 100 \quad (5)$$

#### Where

$P_i$ : is the contribution of factor i to the response;

$b_i$ : the statistical coefficient corresponding to factor i.

For further work, three (3) best zeolite catalysts (CAZ) were selected on the basis of their surface acidity ( $Y_{\text{exp}}$ ). These catalysts were characterized.

#### Catalyst characterization:-

XRD on the three (3) catalysts was performed using an ANCHOR SCAN version "1.0" diffractometer at Ahmed Bello University (ABU) in the Federal Republic of Nigeria. The scan range was 5.02 to 75.97° in 0.02° increments over a period of 29.07 seconds; Cu counterelectrode; 45 kV-40mA.

XRF was carried out using a THERMO-SCIENTIFIC Newton XL3t at the Geology Laboratory of the "Centre d'Excellence Africain en Mines et Environnement Minier (CEA-MEM) at INP-HB, Yamoussoukro, Côte d'Ivoire", to determine the elemental mineralogical composition of the catalyst samples. Measurements in "MINING" mode, in the 2 $\theta$  range for 120 min, were carried out on an accessory fitted with an RFID (Radio Frequency Identification)

chip, enabling the analyzer to detect it automatically and convert it into a benchtop analyzer. A measuring stand called a safety cord is used to prevent the operator from coming into contact with the X-rays emitted by the XRF device. Data transfer was carried out directly on the computer using a powerful reader called Niton XL3t coupled with NDF software. The SAR of the catalysts were obtained using equation (6).

$$SAR = \frac{Si}{Al} = \frac{\%SiO_2 * a_{SiO_2}}{\%Al_2O_3 * a_{Al_2O_3}} \text{ Where } a_{SiO_2} = \frac{M_{Si}}{M_{SiO_2}} \text{ et } a_{Al_2O_3} = \frac{M_{Al_2}}{M_{Al_2O_3}} \quad (6)$$

**Where**

$M_{Si}$  = Molar mass of silicon ;

$M_{Al}$  = Molar mass of aluminium;

$M_{SiO_2}$  = Molar mass of silicon oxide;

$M_{Al_2O_3}$  = Molar mass of aluminum oxide;

$a_{SiO_2}$  = Silicon oxide constant ;

$a_{Al_2O_3}$  = Aluminumoxide constant;

$\%SiO_2$  =  $SiO_2$  content of the sample (obtained by XRF) ;

$\%Al_2O_3$  =  $Al_2O_3$  content of sample (obtained by XRF).

FT-IR was carried out on the catalysts in ATR (Attenuated Total Reflectance) mode using a Bruker Alpha Fourier transform spectrometer equipped with a diamond crystal (refractive index of diamond: 2.451) in the wavelength range from  $400 \text{ cm}^{-1}$  to  $4000 \text{ cm}^{-1}$  with a spectral resolution of  $4.0 \text{ cm}^{-1}$ . Measurements of the textural properties of the three catalysts were determined by the BET method. This was carried out at ABU (Ahmed Bello University) in the Federal Republic of Nigeria, using a Quantachrome Nova Win-Data Acquisition and Reduction for NOVA instruments version 11.03. Catalyst samples were degassed at  $150^\circ\text{C}$  and  $250^\circ\text{C}$  for  $\approx 3$  hours.

Adsorption and desorption processes are monitored by measuring the change in thermal conductivity of a gas stream composed of 99.99% nitrogen (adsorbate) and 70% 99.99% helium (carrier gas). SEM was carried out using the JEOLJ SM-5300. Catalyst samples were pre-coated with a thin layer of gold (between 20 and  $30\text{\AA}$ ) to increase their electrical conductivity. TGA and DTA were carried out at the University of Kaduna in the Federal Republic of Nigeria, using a PerkinElmer TGA-4000 instrument manufactured in the Netherlands.

**Catalytic cracking reaction:-**

**Microreactor characteristics:-**

A microreactor was specially designed for catalytic cracking operations at the ESI (Higher School of Industry) mechanical engineering workshop at INP-HB. The  $10 \text{ cm}^3$  microreactor was obtained using equations (7) and (8):

$$V = S_b * H \quad (7)$$

$$V = \pi * R^2 * H = \pi * \frac{D^2}{4} * H \quad (8)$$

**Where**

Sb: Base area;

H: height of the microreactor (for  $V \approx 9.9 \text{ cm}^3 \approx 10 \text{ cm}^3$ ,  $H \approx 12.5 \text{ cm}$ );

R: Radius of the microreactor (for  $H = 12.5 \text{ cm}$ ,  $R \approx 0.5 \text{ cm}$  and therefore  $D \approx 1 \text{ cm}$ ).

D: Diameter of the microreactor.

As the microreactor is made of steel, which has a melting point between  $1400^\circ\text{C}$  and  $1500^\circ\text{C}$ , it can withstand temperatures above  $500^\circ\text{C}$  and pressures between 1 and 3 bar.

**Description of the cracking plant:-**

Fig. 2 shows the model used for catalytic cracking of naphtha on the three best CAZs: CAZ-1, CAZ-2, and CAZ-7.

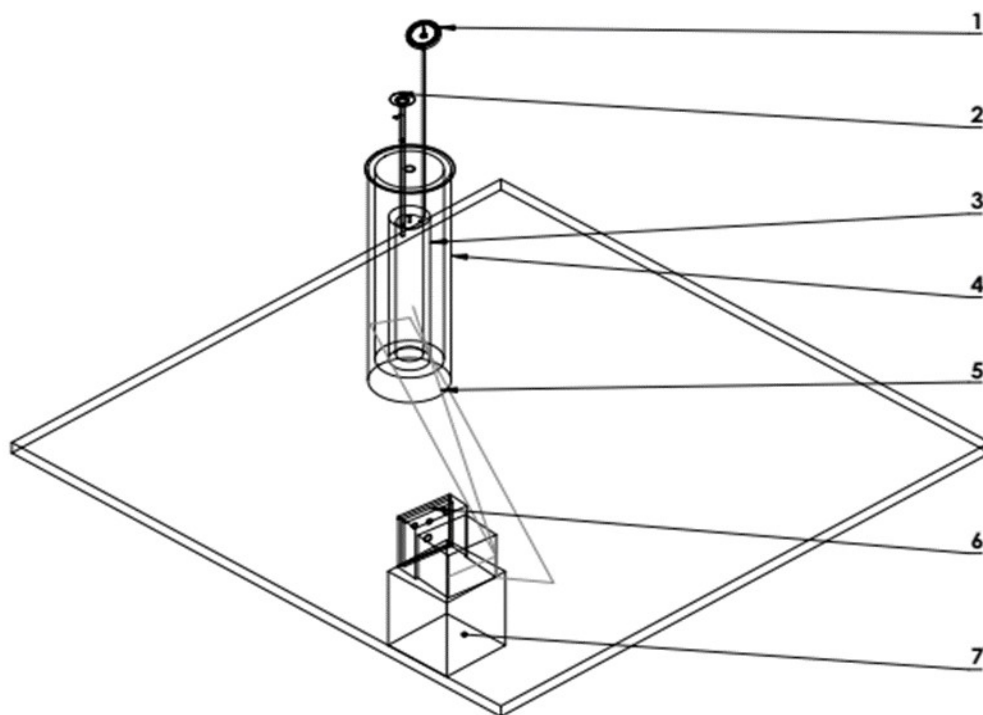


Fig. 2. Model of the cracking plant (Design: SolidWorks software).

- (1): Pressure gauge
- (2): Power supply
- (3): Microreactor
- (4): Oven
- (5): Conductive wire connecting the oven to the temperature controller
- (6): Temperature controller
- (7): Temperature controller support.

**Naphtha cracking occurred under mild conditions. The operating conditions considered were as follows:**

- Reaction temperatures: 250°C;
- pressure: atmospheric (1 atm);
- Residence time: 60s;
- Microreactor quenching time: 1h;
- Spatial velocity (PPH): 1 h<sup>-1</sup> (injection using a syringe).

PPH is defined as the ratio of the feed's mass flow rate to the catalyst's mass (Trambouze, 1999).

#### Cracking procedure:-

To perform the cracking operation, 0.3 g of CAZ is placed in the microreactor. Then, the microreactor is inserted into the electric furnace, and the temperature is raised in 50°C increments until it reaches 250°C. After ensuring the installation is airtight, 5 mL of naphtha (3.06 g) is injected into the microreactor as the feedstock. The oven temperature is controlled using an automatic regulator, and the reactor temperature is monitored with a K/J type probe thermometer. Finally, the cracking products leaving the microreactor are cooled for one hour in cold water at approximately 0°C and then weighed. Note that thermal control cracking (without catalyst) and a repeat reaction (catalytic reaction) were carried out for the catalytic cracking reaction. The  $X_i$  yields (equation (9)) were calculated by dividing the mass of the product obtained after cracking ( $m_0$ ) by the mass introduced into the reactor ( $m_i$ ).

$$X_i = \frac{m_0}{m_i} * 100 \quad (9)$$

The rate of increase of the proportion of light molecules, denoted  $T_a$  (equation (10)), was calculated using the following formula:

$$T_a = \frac{\sum P_d}{\sum P_t} \text{ (10)}$$

**Where**

$P_d$  is the difference in proportions between CT and CC.  $P_t$  is the proportion of all light molecules that have increased. The products obtained after catalytic cracking are characterized by Gas Chromatography-Mass Spectrometry (GC-MS).

**Results and Discussion:-**

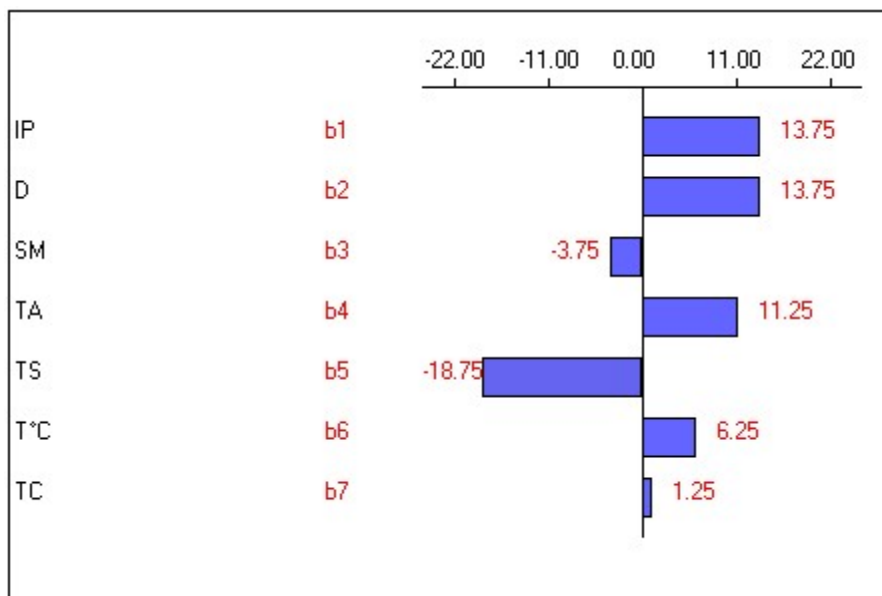
**Plackett-Burman design:-**

Table 4 below shows the experimental design and the  $Y_{exp}$  response values, which were calculated using equation (3). It also shows the experimental error,  $2\sigma_e$ .

**Table .4Experimental results obtained for catalysts according to Hadamard's plan.**

Factors									
N°Exp	CAZ	true values							$Y_{exp}(\text{meq/g})$
		$U_1$ (g)	$U_2$	$U_3$ ( $\mu\text{m}$ )	$U_4$ (h)	$U_5$ (h)	$U_6$ ( $^{\circ}\text{C}$ )	$U_7$ (h)	
1	CAZ-1	2	$D_1$	24	10	12	550	4	65
2	CAZ-2	2	$D_2$	18	10	24	550	3	60
3	CAZ-3	1	$D_2$	24	6	24	650	3	15
4	CAZ-4	1	$D_1$	24	10	12	650	4	50
5	CAZ-5	2	$D_1$	18	10	24	550	4	35
6	CAZ-6	2	$D_2$	18	6	24	650	3	50
7	CAZ-7	1	$D_2$	24	6	12	650	4	55
8	CAZ-8	1	$D_1$	18	6	12	550	3	20
Experimental error $2\sigma_e$		5.76							

Fig. 3 shows the estimated coefficients and their statistics.



**Fig. 3. Estimates and coefficient statistics.**

A significance test was performed on each coefficient in the model based on the criterion that a coefficient is statistically significant if its absolute value is greater than or equal to twice the experimental error (Goupy & Creighton, 2006). The experimental standard deviation  $\sigma_e$  2.88 was determined by repeating the test five times (Exp). Since there are two categories of factors (qualitative and quantitative), the value of the experimental error ( $2\sigma_e$ ) is 5.76. Based on this rule, the significant factors in this experiment are aluminum isopropoxide (IP), clay (D), stirring time (TA), drying time (TS), and calcination temperature ( $T^\circ\text{C}$ ). Sand ( $S_M$ ) and calcination time (TC) are non-significant factors.

As shown in Table 4, surface acidity varies from 15 to 65 milliequivalents per gram (meq/g). By analyzing the significant factors in Fig. 3, we can see that surface acidity is low (15 meq/g) when  $D_2$  clay is used as a matrix with one gram of IP (1 g), a six-hour stirring time, a 24-hour drying time, and a  $650^\circ\text{C}$  calcination temperature. Conversely, using the same  $D_2$  clay with two grams of IP, a stirring time of ten hours, a drying time of twenty-four hours, and a calcination temperature of  $550^\circ\text{C}$  results in higher surface acidity (65 meq/g). This improvement in surface acidity (15 meq/g to 60 meq/g) could be explained not only by the amount of IP used, but also by the stirring time. Conversely, the surface acidity is low (20 meq/g) when using raw clay  $D_1$  as a matrix with one gram of IP, a six-hour stirring time, a 12-hour drying time, and a  $550^\circ\text{C}$  calcination temperature. However, when using the same raw clay  $D_1$  with two grams (2g) of aluminum isopropoxide (IP), a stirring time of 10 hours, a drying time of 12 hours, and a calcination temperature of  $550^\circ\text{C}$ , the surface acidity becomes very high (65 meq/g). This increase in surface acidity (from 20 meq/g to 65 meq/g) could also be explained by the difference in the amount of IP used and the stirring time.

The surface acidity values in Table 4 are similar to those reported by Oumarou et al. (2021), but significantly higher than the values of FCC zeolite catalysts (30 to 50 meq/g) reported by Ibarra et al., (Ibarra et al., 2019). These recorded values were also compared with those of an industrial catalyst used by the Zinder Refining Company (SORAZ). The CAZ-1, CAZ-2, CAZ-4, CAZ-6, and CAZ-7 catalysts are superior in terms of surface acidity to the industrial catalysts used by SORAZ, which have a surface acidity of 40 meq/g. Ultimately, to obtain a more active zeolite catalyst, depending on whether  $D_1$  or  $D_2$  is used as the synthesis support, it would be preferable to use two grams (2 g) of IP as an additive and a stirring time of 10 hours. Additionally, 24  $\mu\text{m}$  sand, a 12-hour drying time, a  $550^\circ\text{C}$  calcination temperature, and a 4-hour calcination time would suffice.

Fig. 4 shows how the various factors contribute to the recorded  $Y_{\text{exp}}$  response.

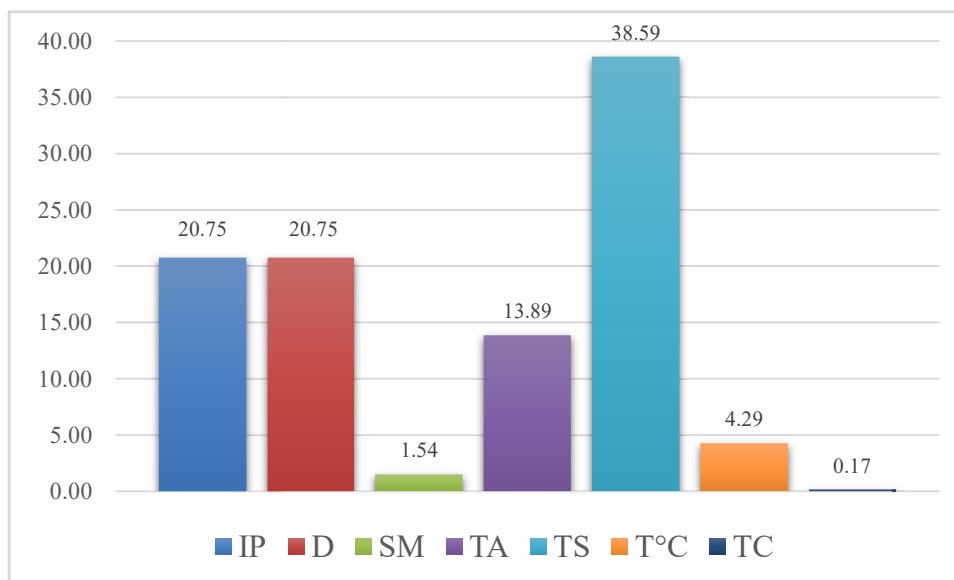


Fig. 4. Contribution of Various Factors

Fig. 4 illustrates the impact of various factors on the acidity of the synthesized catalysts' surfaces. The contributions of aluminum isopropoxide (IP), clay (D), Goulbi-Maradi sand ( $S_M$ ), stirring time (TA), drying time (TS), calcination temperature ( $T^\circ\text{C}$ ), and calcination time (TC) to surface acidity are 20.75, 20.75, 1.54, 13.89, 38.59, 4.28, and 0.17, respectively. For the next stage of this study, the three best catalysts (CAZ-1, CAZ-2, and CAZ-7) were selected

based on surface acidity. The catalysts were characterized using XRD, XRF, FT-IR, BET, SEM, and DTA-TGA methods.

### Characteristics of CAZ-1, 2, and 7 Catalysts:-

#### X-ray diffraction (XRD):-

Fig. 5 below shows the XRD analysis results for the three catalysts.

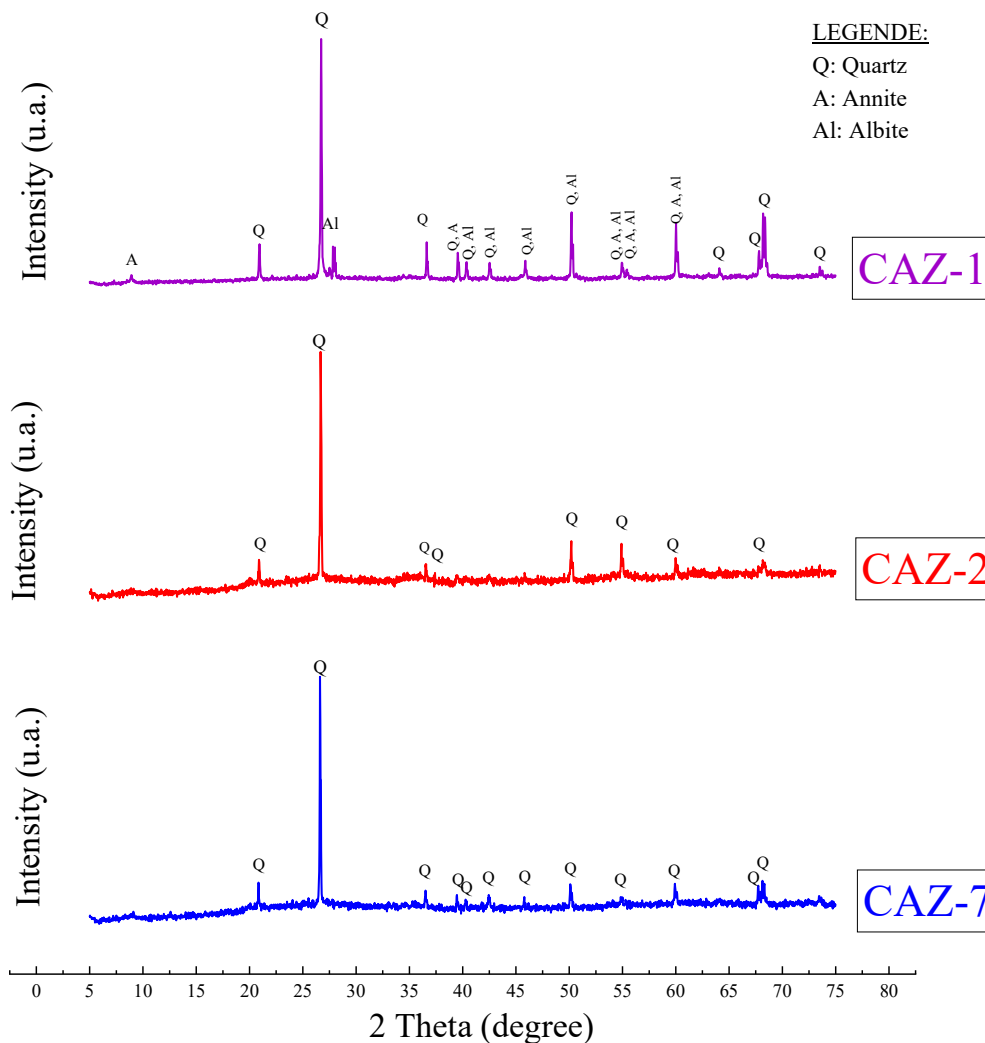


Fig. 5. X-ray diffractogram of CAZ-1, CAZ-2 and CAZ-7 catalysts.

Observing the diffractograms of the three catalysts (Fig. 5) reveals the disappearance of all the characteristic peaks of kaolinite (Abdourahamane et al., 2022) and confirms their transformation into métakaolinite (Zibouche et al., s. d., 2009). According to K. Traoré (Traore, 2003), at temperatures above 500°C, kaolinite ( $\text{Al}_2\text{O}_3 \cdot 2\text{SiO}_2 \cdot 2\text{H}_2\text{O}$ ) loses its hydroxyl (OH) function and transforms into metakaolinite ( $\text{Al}_2\text{O}_3 \cdot 2\text{SiO}_2$ ). The transformation of kaolinite into metakaolinite (metakaolinitization) can be explained by the fact that the catalysts were calcined prior to XRD analysis. The results of the experimental plan indicate that CAZ-1 and CAZ-2 were calcined at 550°C, while CAZ-7 was calcined at 650°C. However, according to authors Murat and A. Bachiorrini (Murat & Bachiorrini, 1982), the metakaolinite phase is the most reactive in the series of thermal transformations of kaolinite. These destroyed clay

minerals give way to peaks characteristic of quartz ( $\text{SiO}_2$ ). This can be explained by the effective incorporation of silica ( $\text{SiO}_2$ ) during the synthesis of the catalysts.

Observation of the diffractograms of the three catalysts reveals intense, well-resolved peaks. For CAZ-1, the peaks appear around  $21.07^\circ$ ,  $26.67^\circ$ , and  $36.80^\circ$ . For CAZ-2, the peaks appear around  $20.80^\circ$ ,  $26.67^\circ$ , and  $36.55^\circ$ . For CAZ-7, the peaks are visible at  $20.82^\circ$ ,  $26.67^\circ$ , and  $36.55^\circ$ . These intense peaks are similar to those of standard, perfectly crystalline Y zeolite (100% crystallinity), as analyzed by XRD in the range of  $5.018^\circ(2\theta)$  to  $69.966^\circ(2\theta)$  with a step size of  $0.026^\circ$ . This highly crystalline zeolite standard exhibits peak intensities characteristic of reflections 511, 440, and 642, which correspond to  $20.5^\circ$ ,  $26.5^\circ$ , and  $35^\circ$ , respectively (Qin et al., 2011). The peaks of the highly crystalline standard zeolite are similar to the intense, well-resolved peaks of our three synthesized zeolite catalysts (CAZ-1, CAZ-2, and CAZ-7).

#### X-ray fluorescence (XRF):-

The three best synthesized CAZ-1, CAZ-2, and CAZ-7 catalysts were analyzed using the XRF method. The results are grouped in Table 5.

**Table.5 Chemical composition,  $\text{SiO}_2/\text{Al}_2\text{O}_3$  and Si/Al ratios of CAZ-1, 2 and 7.**

Oxides (%)	CAZ-1	CAZ-2	CAZ-7
$\text{SiO}_2$	74.67	64.94	65
$\text{Al}_2\text{O}_3$	12.16	17.19	17.65
$\text{Fe}_2\text{O}_3$	3.44	8.35	7.62
MgO	2.88	2.98	1.94
$\text{P}_2\text{O}_5$	0.22	0.18	0.19
$\text{SO}_3$	0.21	0.05	0.05
$\text{TiO}_2$	0.66	0.76	0.73
MnO	0.29	0.47	0.44
CaO	0.60	1.21	1.10
$\text{K}_2\text{O}$	1.17	0.89	0.78
$\text{Na}_2\text{O}$	0.85	0.45	0.39
$\text{ZrO}_2$	0.14	0.03	0.03
Autres	2.71	2.5	4.08
<b><math>\text{SiO}_2/\text{Al}_2\text{O}_3</math></b>	<b>6.14</b>	<b>3.77</b>	<b>3.68</b>
<b>Si/Al</b>	<b>5.33</b>	<b>3.27</b>	<b>3.19</b>

As shown in Table 5, there was a considerable increase in  $\text{SiO}_2$  content and a significant decrease in  $\text{Al}_2\text{O}_3$  content across all catalyst samples.  $\text{SiO}_2$  content increased from 58.851% in the  $\text{D}_1$  zeolite catalyst synthesis support to 74.67% in CAZ-1. Similarly, it increased from 42.88% in  $\text{D}_2$  to 64.94% in CAZ-2 and 65% in CAZ-7. This increase can be attributed to the addition of  $\text{S}_M$  sand ( $\text{SiO}_2$ ) during zeolite catalyst synthesis. According to the work of (Otmani, 2006), silica confers good mechanical strength (Otmani, 2006) to catalysts and increases their acidity (P. Leprince, s. d.) for catalytic cracking operations. Furthermore, the  $\text{SiO}_2$  content of all the synthesized catalysts (CAZ-1, CAZ-2, and CAZ-7) is higher than that of the commercial fluid catalytic cracking (FCC) catalyst ( $\text{SiO}_2 = 54.1\%$ ) used by Hussain et al. (2015) (Hussain et al., 2016) in the catalytic cracking of vacuum gas oil, as well as that of the ZSM-5 catalysts ( $\text{SiO}_2 = 57.12\%$ ) synthesized by Y. Ghrib et al. (2015) (Ghrib et al., 2017) from metakaolinite.

The  $\text{SiO}_2$  and  $\text{Al}_2\text{O}_3$  contents result in silica alumina ratios (SAR) of 5.33 for CAZ-1, 3.27 for CAZ-2, and 3.19 for CAZ-7. CAZ-1's SAR falls within the Y zeolite range (Si/Al: 3.5–5.5) (Chester & Derouane, 2009), while CAZ-2's and CAZ-7's SARs fall within the intermediate Y zeolite range (Si/Al: 2–5) (Breck, 1973).

#### Fourier Transform Infrared Spectroscopy (FT-IR):-

FT-IR was performed to detect chemical functions on the surfaces of three zeolite catalysts. The observed bands were assigned using data from the literature. The results of this analysis are shown in Fig. 6.

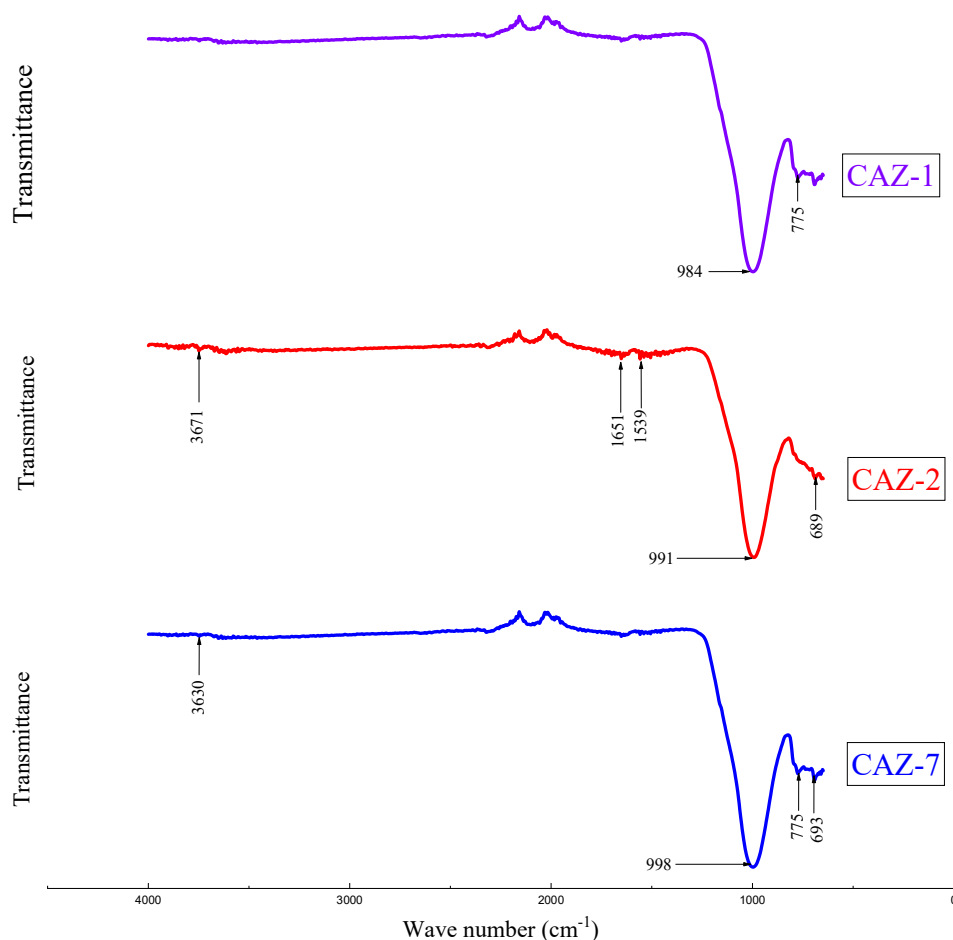


**Fig. 6.** FT-IR spectrum of CAZ-1, CAZ-2 and CAZ-7 catalysts from 4000 to 400  $\text{cm}^{-1}$ .

Fig. 6 shows the FT-IR spectra of the three synthesized zeolite catalysts: CAZ-1, CAZ-2, and CAZ-7. The FT-IR spectra of CAZ-2 and CAZ-7 show bands appearing at 689 and 693  $\text{cm}^{-1}$ , respectively. These bands are attributed to the stretching vibrations of the symmetric and asymmetric T-O-T (T = Si or Al) bonds of the internal tetrahedra ( $\text{SiO}_4$  and  $\text{AlO}_4$ ) of the CAZ-2 and CAZ-7 catalysts (Bouna et al., 2020). According to Ahmad Asghari et al. (2019), this T-O-T structure is specific to zeolite catalysts (Asghari et al., 2019).

The bands that appear at 775  $\text{cm}^{-1}$  on the FT-IR spectra of CAZ-1 and CAZ-7 are attributed to the stretching of the framework of the siliceous materials and the conversion of the octahedral coordination of kaolinite ( $\text{Al}^{3+}$ ) to the tetrahedral coordination of métakaolinite (Gonçalves et al., 2008; Percival et al., 1974a). This conversion is explained by the temperature and calcination time during synthesis of these zeolite catalysts (Yue et al., 2020). The peaks at 984  $\text{cm}^{-1}$  on the FT-IR spectrum of CAZ-1, 991  $\text{cm}^{-1}$  on the FT-IR spectrum of CAZ-2, and 998  $\text{cm}^{-1}$  on the FT-IR spectrum of CAZ-7 correspond to aluminosilicate vibrations (Percival et al., 1974b). The shoulder peaks appearing at 1539 and 1651  $\text{cm}^{-1}$  on the FT-IR spectrum of CAZ-2 are attributed to stretching of the external asymmetry of the Si-O-Si bond. The bands observed at 3671 and 3630  $\text{cm}^{-1}$  on the FT-IR spectra of CAZ-2 and CAZ-7, respectively, are related to the stretching vibrations of the hydroxyl groups (Al-OH) on the inner surface and the stretching vibrations of the inner hydroxyl groups (Asghari et al., 2019; Yang et al., 2012).

**Specific surface area, pore volume and pore diameter of CAZ:-**

The specific surface areas ( $S_{\text{BET}}$ ,  $S_{\text{micro}}$  and  $S_{\text{meso}}$ ), pore volumes ( $V_{\text{micro}}$  and  $V_{\text{meso}}$ ) and pore diameters ( $D_{\text{micro}}$  and  $D_{\text{meso}}$ ) of the three best catalysts (CAZ-1, CAZ-2 and CAZ-7) synthesized were evaluated. The BET specific surface area ( $S_{\text{BET}}$ ) was evaluated using the BET method, and the specific surface areas of micropores ( $S_{\text{micro}}$ ) and mesopores ( $S_{\text{meso}}$ ) and the volume of micropores ( $V_{\text{micro}}$ ) were evaluated using the t-plot method. The mesopore volumes ( $V_{\text{meso}}$ ) and mesopore diameters ( $D_{\text{meso}}$ ) were evaluated using the BJH method. The micropore diameter ( $D_{\text{micro}}$ ) was evaluated using the HK method. Micropore diameter ( $D_{\text{micro}}$ ) was assessed using the HK method. The experimental results of all these analyses are presented in the following Table 6.

**Table. 6 Specific surface area, pore volume and pore diameter of CAZ-1, 2 and 7.**

CAZ	$S_{\text{BET}}$ ( $\text{m}^2/\text{g}$ )	Surface Spécifique		Volume des pores		Diamètre des pores	
		$S_{\text{micro}}$ ( $\text{m}^2/\text{g}$ )	$S_{\text{meso}}$ ( $\text{m}^2/\text{g}$ )	$V_{\text{micro}}$ ( $\text{cm}^3/\text{g}$ )	$V_{\text{meso}}$ ( $\text{cm}^3/\text{g}$ )	$D_{\text{micro}}$ (nm)	$D_{\text{meso}}$ (nm)
CAZ-1	190.04	195.20	190	0.02	0.09	1.84	2.15
CAZ-2	260.90	299.30	260.90	0.04	0.16	0.36	2.14
CAZ-7	322	346.80	322	0.05	0.17	1.84	2.13

The results show that the specific surface areas ( $S_{\text{BET}}$  and  $S_{\text{meso}}$ ) of CAZ-2 and CAZ-7 are equal after synthesis. However, they increased during alkaline treatment with NaOH, the addition of sand ( $S_{\text{M}}$ ), and the addition of aluminum isopropoxide (IP), as well as during calcination. Based on the  $D_2$  support used for the synthesis of CAZ-2 and 7 (256.30  $\text{m}^2/\text{g}$ ), the  $S_{\text{BET}}$  and  $S_{\text{meso}}$  increased from 256.30 to 260.90  $\text{m}^2/\text{g}$  and from 256.30 to 322  $\text{m}^2/\text{g}$ , respectively. According to L. J. He *et al.*, 2017 (Department of Chemistry and Chemical Engineering, Hunan Institute of Science and Technology, Yueyang 414 006, Hunan, P.R. China *et al.*, 2017) and Z. Zhang *et al.*, 2014 (Z. Zhang *et al.*, 2014), this increase reflects an increase in mesoporousness during synthesis, which can be explained by an increase in calcination temperature. The development of microporosity in CAZ-2 and CAZ-7 can be explained by an increase in the specific surface area of micropores ( $S_{\text{micro}}$ ). Thus, the specific surface areas of micropores ( $S_{\text{micro}}$ ) increase from 260.90  $\text{m}^2/\text{g}$  to 299.30  $\text{m}^2/\text{g}$  for CAZ-2, and those of mesopores ( $S_{\text{meso}}$ ) increase from 322.00  $\text{m}^2/\text{g}$  to 346.80  $\text{m}^2/\text{g}$  for CAZ-7. Furthermore, these specific surface area results for the CAZ-2 and CAZ-7 catalysts are higher than those for the commercial FCC catalysts used by Ribeiro *et al.*, 2013 (Ribeiro *et al.*, 2013) in their work evaluating the efficiency of commercial FCC catalysts. Similarly, the specific surface area results for our CAZ-2 and CAZ-7 catalysts are higher than those obtained by Y. Yue *et al.*, 2018 ( $S_{\text{BET}} = 292 \text{ m}^2/\text{g}$ ,  $S_{\text{micro}} = 224 \text{ m}^2/\text{g}$ , and  $S_{\text{meso}} = 68 \text{ m}^2/\text{g}$ ) when synthesizing ZSM-5 zeolite catalysts using silicon-rich diatomite and aluminum-rich rectorite (Yue *et al.*, 2018). However, the specific surface area of CAZ-1 decreased considerably after synthesis from 446.50  $\text{m}^2/\text{g}$  ( $D_1$ ) to a virtually constant value ( $S_{\text{BET}} = 190.04 \text{ m}^2/\text{g}$ ,  $S_{\text{micro}} = 195.20 \text{ m}^2/\text{g}$ , and  $S_{\text{meso}} = 190.00 \text{ m}^2/\text{g}$ ). This can be explained by the presence of impurities (carbonates, organic matter, etc.) in the  $D_1$  synthesis medium of CAZ-1 catalysts, as reported by E.A. Amam (Emam, 2013).

A comparable trend to that of the specific surface areas of CAZ-2 and CAZ-7 was observed for the mesopore diameter ( $D_{\text{meso}}$ ) and micropore diameter ( $D_{\text{micro}}$ ) diameters of the same catalysts. Thus,  $D_{\text{meso}}$  increased from 2.13 nm (CAZ-7) with a hydrothermal treatment time of 6 hours to 2.14 nm (CAZ-2) with a treatment time of 10 hours. However, the micropore diameter of the CAZ-2 and CAZ-7 catalysts decreased from 1.84 nm (CAZ-7) after 6 hours to 0.36 nm (CAZ-2) after 10 hours. I. Qoniah *et al.*, 2015 also observed an increase in mesopore diameter and a decrease in micropore diameter as a function of stirring time in their work on the direct synthesis of mesoporous ZSM-5 zeolite catalysts using kaolinite clay from Indonesia (Qoniah *et al.*, 2015). This shows that a long period of hydrothermal treatment promotes the formation of mesoporous structures in the framework of zeolite catalysts (Enterría *et al.*, 2014).

Similar to the  $D_{\text{micro}}$  of CAZ-2 and CAZ-7, a trend was observed in the mesopore volume ( $V_{\text{meso}}$ ) and micropore volume ( $V_{\text{micro}}$ ) volumes of the CAZ-2 and CAZ-7 catalysts. Thus,  $V_{\text{meso}}$  decreased from  $0.17 \text{ cm}^3/\text{g}$  (CAZ-7) with a 6-hour hydrothermal treatment to  $0.16 \text{ cm}^3/\text{g}$  (CAZ-2) with a 10-hour hydrothermal treatment. The  $V_{\text{micro}}$  of the catalysts decreased slightly, from  $0.05 \text{ cm}^3/\text{g}$  (CAZ-7) at 6 hours to  $0.04 \text{ cm}^3/\text{g}$  (CAZ-2) at 10 hours. H. Jia et al., 2021 (Jia et al., 2021); also observed a decrease in the volume of micropores during their work on the hydrothermal synthesis of ZSM-5 zeolite catalysts.

#### Scanning Electron Microscopy (SEM):-

SEM was performed on the three (3) zeolite catalysts (CAZ-1, CAZ-2, and CAZ-7). The images obtained are shown in Figs. 7(a), 7(b) and 7(c) for CAZ-1, CAZ-2 and CAZ-7, respectively.

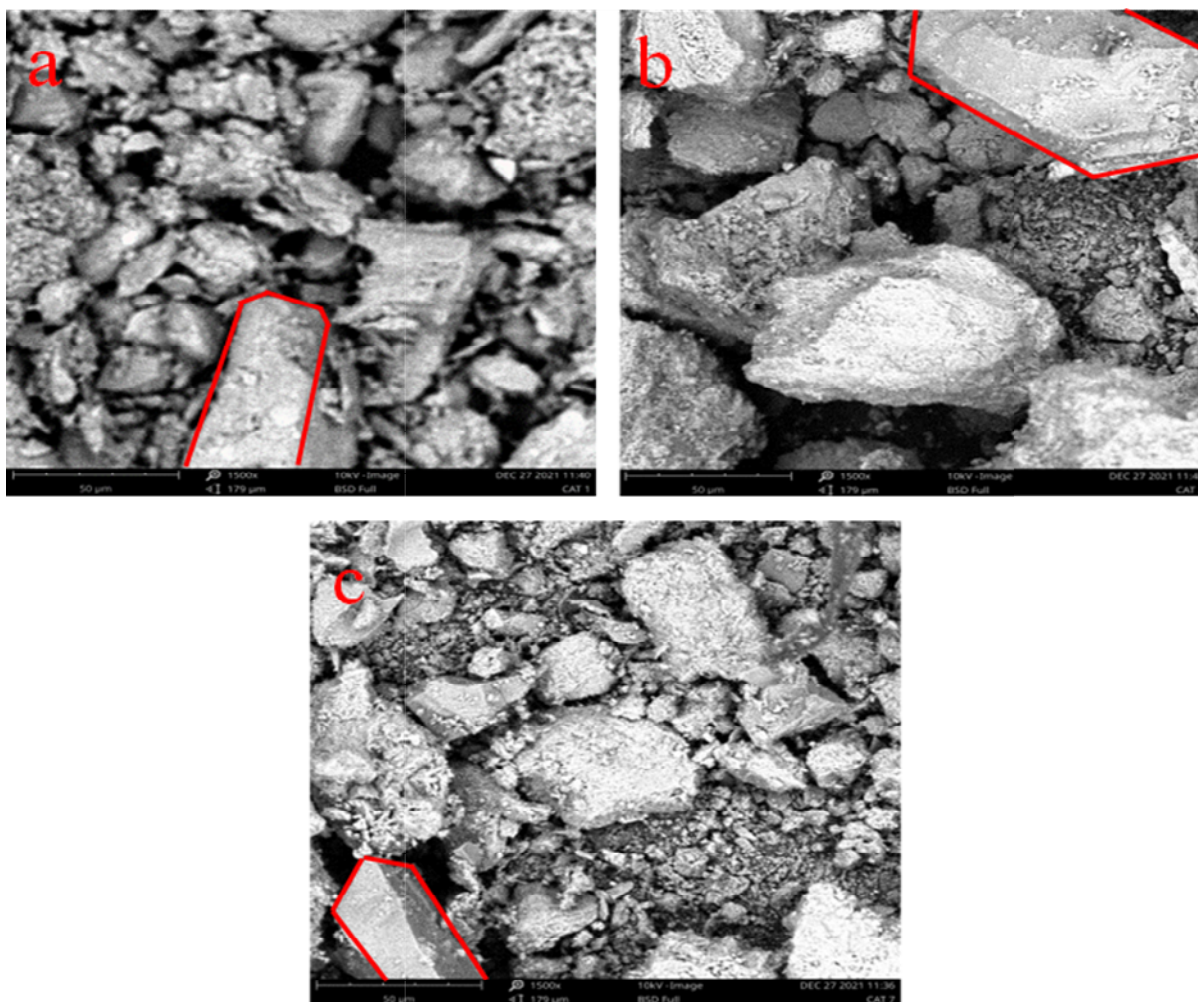


Fig. 7. SEM images of CAZ-1 (a), 2 (b) and 7 (c) at  $50\mu\text{m}$  magnification.

Fig. 7 shows scanning electron microscope (SEM) images of three zeolite catalysts: CAZ-1, CAZ-2, and CAZ-7. All three catalysts—CAZ-1 (Fig. 7a), CAZ-2 (Fig. 7b), and CAZ-7 (Fig. 7c) feature tetrahedra ( $\text{TO}_4$ ) and hexagonal prisms, which are characteristic of Y-type zeolite catalyst morphology (Jia et al., 2021; Kovo et al., 2009). These structures contribute to the formation of  $\alpha$ -cavities (supercages) and  $\beta$ -cavities (sodalites), which are specific to Y zeolite (Costa, 2019). The crystallinity of CAZ-1, CAZ-2, and CAZ-7 reached a level similar to that of Y zeolite, which has a highly crystalline structure, i.e., well-defined tetrahedral and/or prismatic crystals (Youssef et al., 2008). This is due to a fairly favorable stirring time (hydrothermal synthesis), which is 10 hours for CAZ-1 and CAZ-2 and 6 hours for CAZ-7 (Table 4). This is in line with the observations of A.S. Kovo et al., 2009 (Kovo et al., 2009), who reported that no zeolite catalyst formation can be obtained after three (3) hours of crystallization. This indicates that CAZ formation has not begun. Using stirring times longer than three hours (six and ten hours) during the synthesis

of our three zeolite catalysts produced well-crystallized catalysts comparable to the highly crystalline standard Y zeolite model.

#### Gravimetric Thermal Analysis (TGA)/Differential Thermal Analysis (DTA):-

To study the thermochemical behavior of the synthesized CAZ-1, CAZ-2, and CAZ-7, Differential Thermal Analysis (DTA) and Gravimetric Thermal Analysis (TGA) were performed. Figs 8, 9, and 10 below show the DTA and TGA results obtained with CAZ-1, CAZ-2, and CAZ-7.

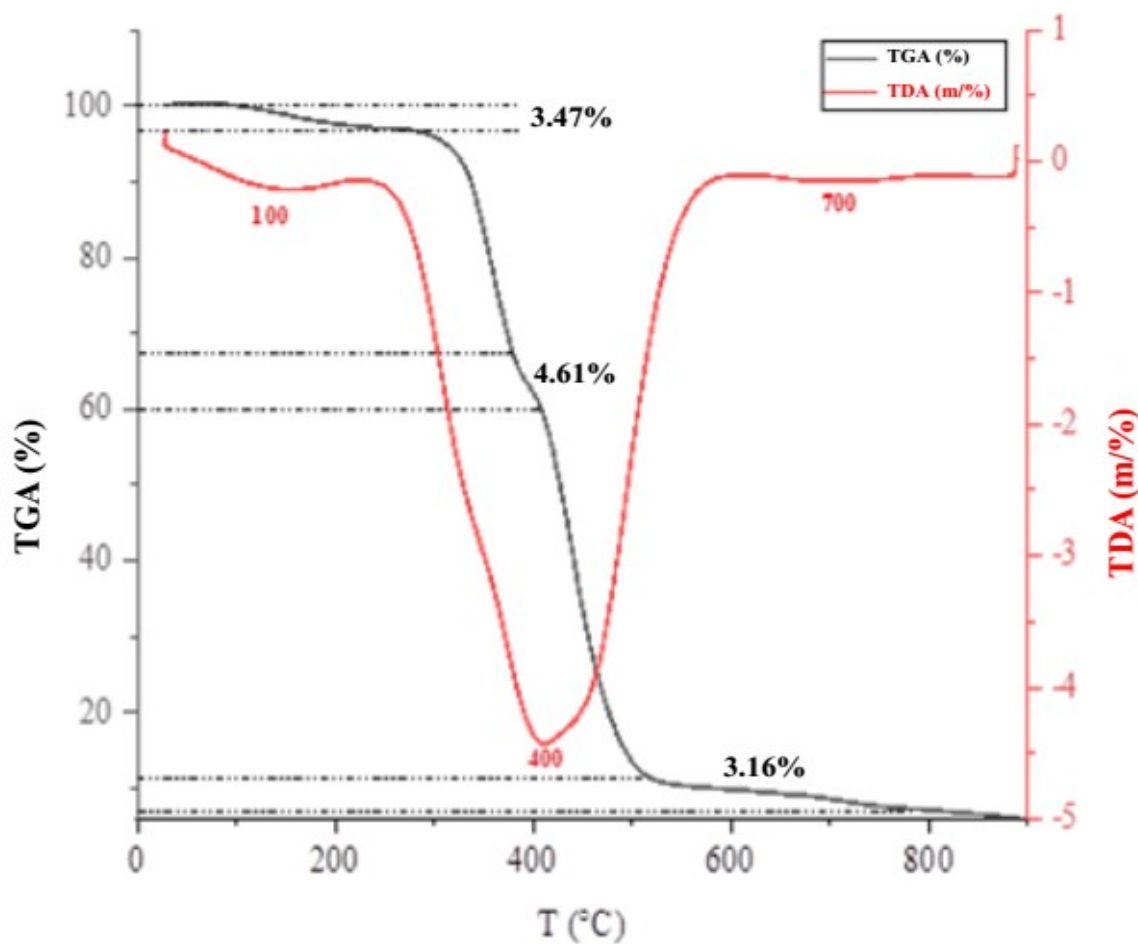


Fig. 8. DTA and TGA curves for CAZ-1.

Fig. 8 corresponds to the DTA isotherm of CAZ-1 and shows three main peaks. A first moderately intense endothermic peak around 100°C, which could indicate the elimination of water by physisorption in the micropores and mesopores of CAZ-1. At this temperature, CAZ-1 experiences a mass loss of approximately 3.47%. A second, very intense endothermic peak occurs around 400°C and is attributable to the dihydroxylation of clay minerals. The mass loss value for CAZ-1 at this temperature is 4.61%. A third, less intense peak appears around 700°C, corresponding to the structural reorganization of CAZ-1. The associated mass loss value is 3.16%.

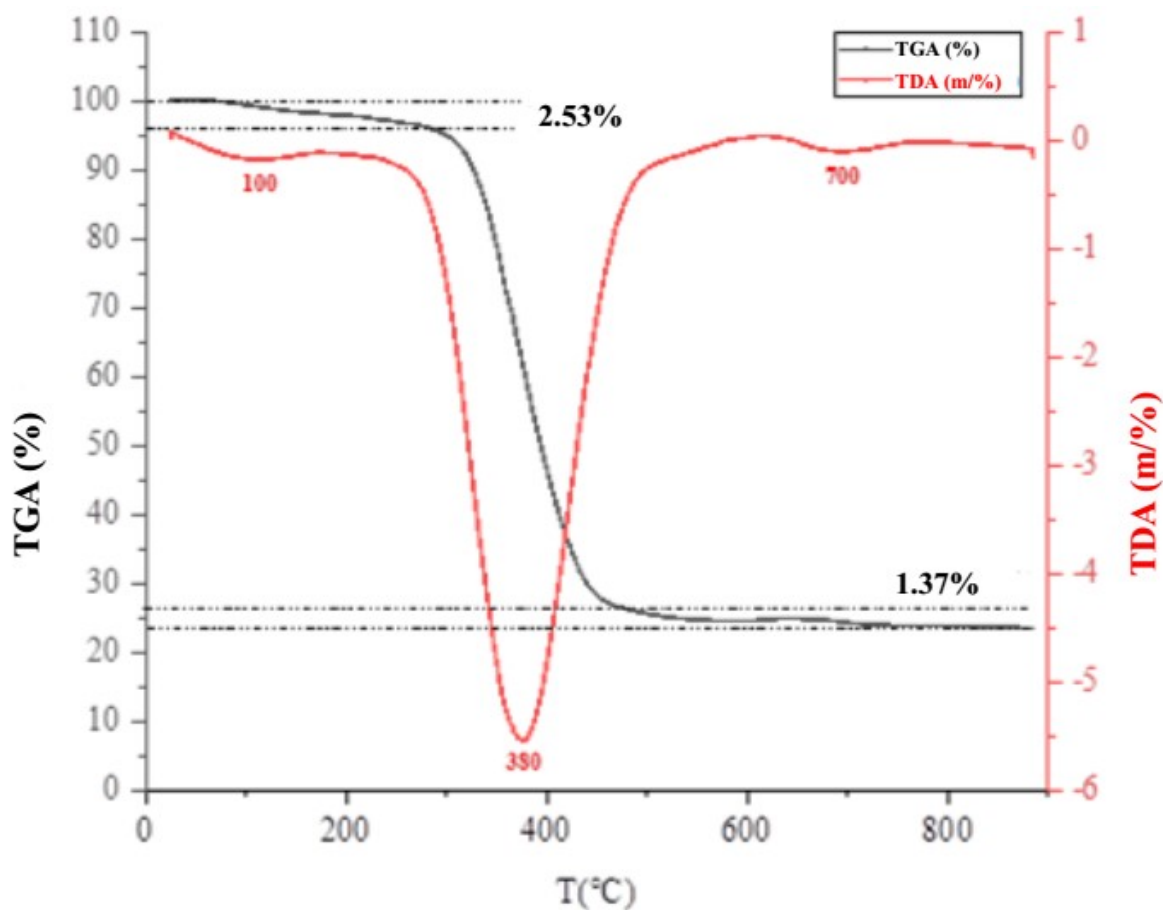


Fig. 9.DTA and TGA curves for CAZ-2.

Fig. 9 illustrates the DTA isotherm of CAZ-2 and shows three endothermic peaks. The first is observed at around 100°C, is moderately intense, and also corresponds to the elimination of water by physisorption in the micro- and mesopores of CAZ-2. At this temperature, CAZ-2 experiences a mass loss of approximately 2.53%. A second, intense peak around 380°C reflects the dihydroxylation of clay minerals, such as kaolinite and illite. The mass loss value for CAZ-2 at this temperature is nearly zero. A third, moderately intense peak around 700°C corresponds to the structural reorganization of CAZ-2. The associated mass loss value for CAZ-2 is 1.37%.

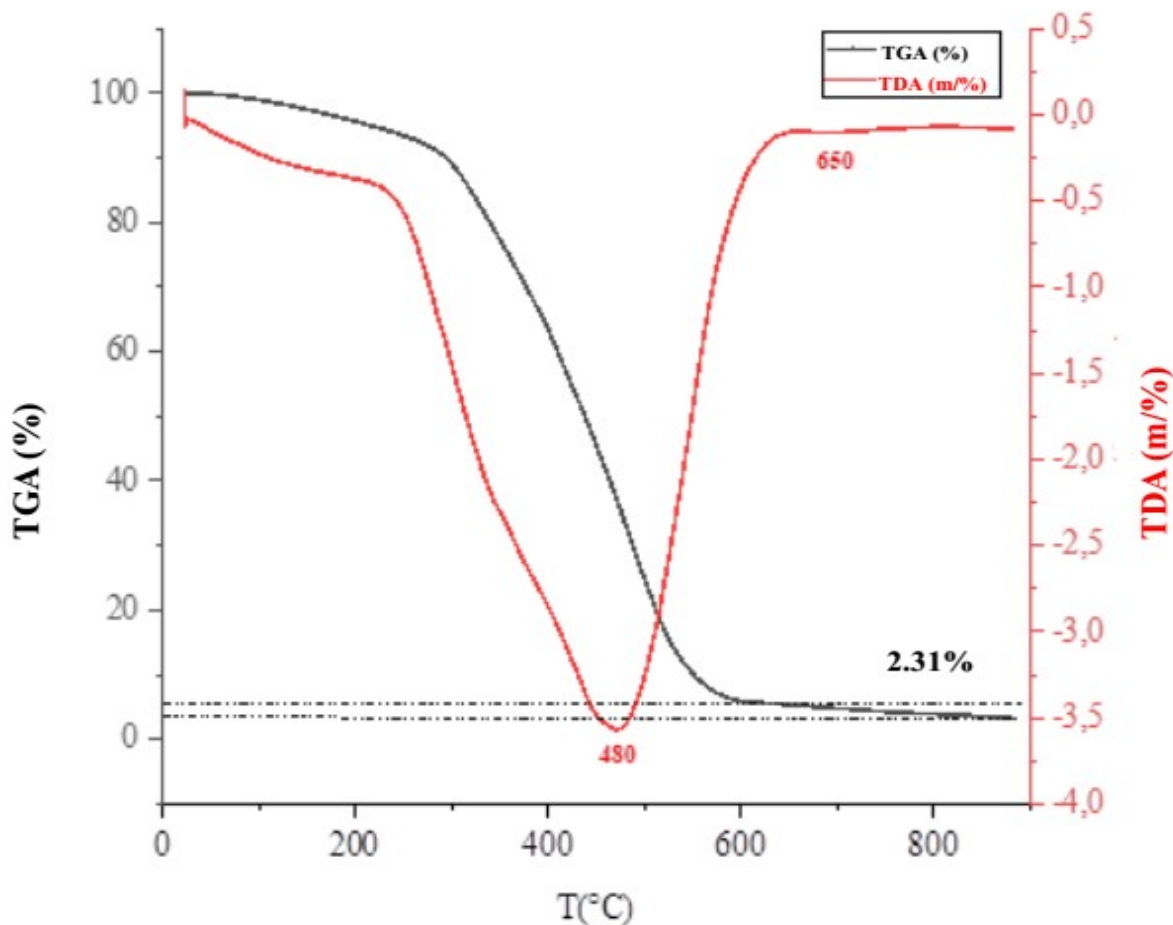


Fig. 10.DTA and TGA curves for CAZ-7.

Fig. 10 shows the DTA isotherm curve for CAZ-7. Two peaks are visible: the first is an intense endothermic peak at approximately 480°C, which is due to dihydroxylation. The mass loss value for CAZ-7 at this temperature is virtually zero. A second, less intense peak around 650°C reflects the structural reorganization of CAZ-7. The associated mass loss value for CAZ-7 is 2.31%. The TGA analysis results obtained for the synthesized zeolite catalysts are similar to those reported by Kabalan (2016) (Kabalan, s. d.) in his thesis on synthesizing nanoporous materials for molecular decontamination and energy storage.

#### Rate of Increase in Light Molecule Proportions, Catalytic Yield, and Reaction Mechanism of Catalytic Cracking with CAZ-1, 2, and 7:-

Table 7 shows the percentage increase in the proportion of light molecules ( $T_a$  (%)), Percent catalytic yields of catalysts 1, 2, and 7 ( $R_{CAZ-1, 2 \text{ et } 7}$ ).

Table .7The proportion of increase rates of molecules and catalytic cracking yields increases in the presence of CAZ-1, CAZ-2, and CAZ-7.

CAZ	variation in proportions		Yield	Explanation
	Light molecules whose proportions have increased.	$T_a$ (%)		
CAZ-1	Cyclohexane, 2-methylhexane, 3-methylhexane, etc.	5	69.93%	Decrease: 5,6-dimethylundecane (13-CA).
CAZ-2	N-octane, 2,2-dimethylheptane, etc.	10.85	83	Decrease: 3,5,5-trimethyl-1-hexene (11-CA).
CAZ-7	5,6-Dimethylundecane, methylheptane, etc.	8.70	50.6	Decrease: 2,6-Dimethylnonane (11-CA)

### CA : Carbon Atom.

It should be noted that CAZ-1 catalysts promoted a 5% increase in light molecules ( $T_a$ ) through the catalytic cracking of naphtha. These molecules include those with six carbon atoms, such as cyclohexane, and those with seven carbon atoms, such as 2-methylhexane, 3-methylhexane, and n-heptane. However, CAZ-1 reduces longer molecules, such as 5,6-dimethylundecane, which has thirteen carbon atoms. This can be explained by the reaction mechanism shown in Fig. 11. The n-hexane molecule undergoes dehydrocyclization (Chester, 1984) to produce cyclohexane. The naphtha cracking yield in the presence of CAZ-1, denoted  $R_{CAZ-1}$ , is 69.93%.

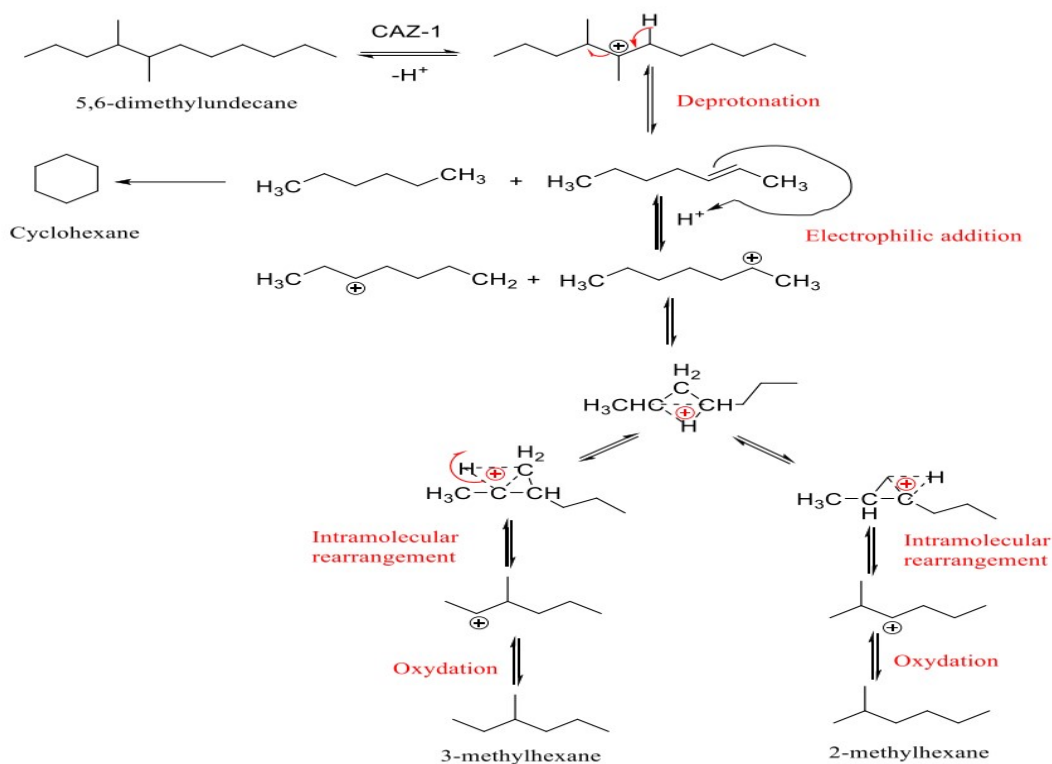
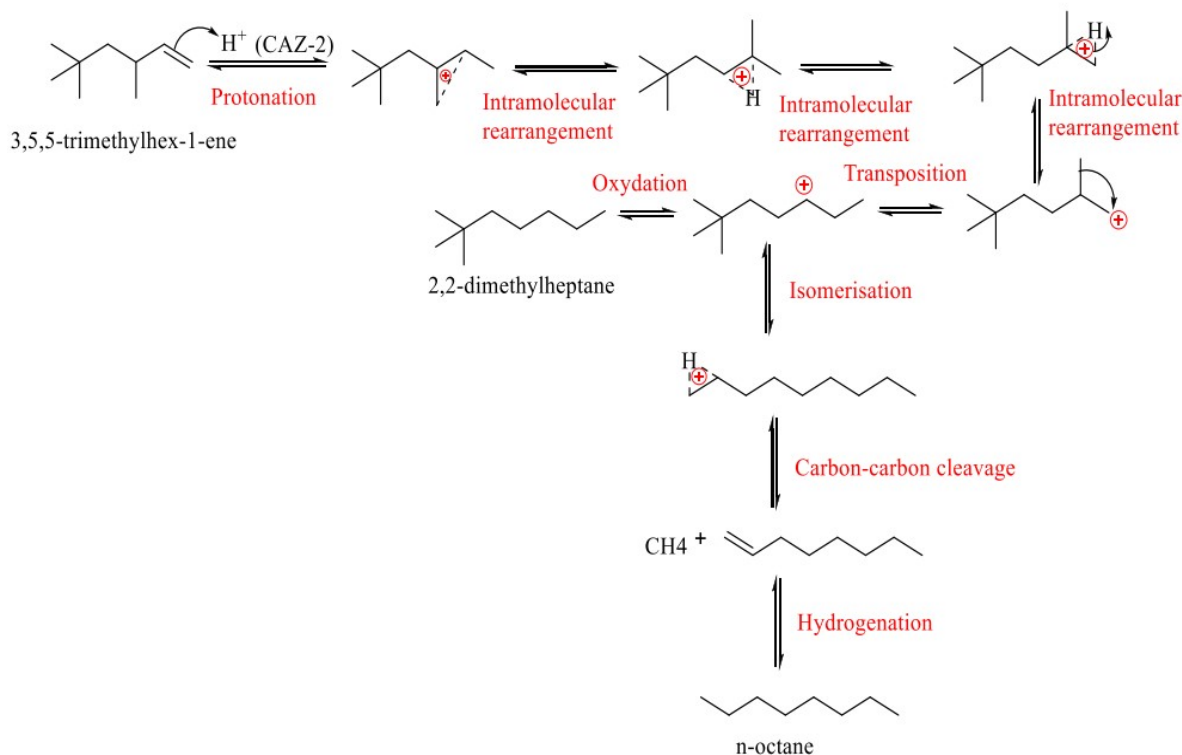


Fig. 11. A proposal for a reaction mechanism to obtain 2-methylhexane, 3-methylhexane and cyclohexane from 5,6-dimethylundecane, using CAZ-1 as a catalyst.

CAZ-2 influences the catalytic cracking of naphtha, increasing the percentage of light molecules to 10.85%. As well as increasing the percentage of light molecules with six (cyclohexane) and seven (2-methylhexane, 3-methylhexane and n-heptane) carbon atoms, CAZ-2 also induced an increase in molecules with eight (n-octane) and nine (2,2-dimethylheptane) carbon atoms. This increase is likely due to a decrease in the percentage of a molecule with eleven (11) carbon atoms: 3,5,5-dimethyl-1-hexene. This phenomenon can be explained by the reaction mechanism shown in Fig. 12. The cracking yield in the presence of CAZ-2 (denoted  $R_{CAZ-2}$ ) is 83%.



**Fig. 12. A proposal for a reaction mechanism to obtain 2,2-dimethylheptane and n-octane from 3,5,5-trimethyl-1-hexene, using CAZ-2 as a catalyst.**

Similar to CAZ-1 and CAZ-2, CAZ-7 impacted the catalytic cracking of naphtha, increasing the proportion of light molecules to 8.70%. Unlike CAZ-1 and CAZ-2, which promoted a decrease in the proportion of 5,6-dimethylundecane, CAZ-7 promoted an increase in this molecule's percentage. The reaction mechanism (Fig. 13) below would explain the increases in 5,6-dimethylundecane and 3-methylheptane from 2,6-dimethylnonane. This mechanism was proposed based on several mechanisms found in the literature. The 2,6-dimethylnonane molecule undergoes protonation (proton transfer from CAZ-1 to the molecule), resulting in a carbocation ion. This ion then undergoes C-C bond cleavage to produce 3-methylheptane (formed via rapid rearrangement through alkyl skipping from 4-methylheptane) and an allylic carbocation ion. This ion then donates a proton to CAZ-7 (deprotonation), forming propene. The propene then undergoes further protonation to form propane. The propane then undergoes isomerisation with the n-decane molecule in the reaction medium to form n-tridecane. The latter undergoes very rapid rearrangement via alkyl jumps (or hydride jumps) to form 5,6-dimethylnonane. The yield of catalytic cracking in the presence of CAZ-7 ( $R_{CAZ-7}$ ) is 50.62%.

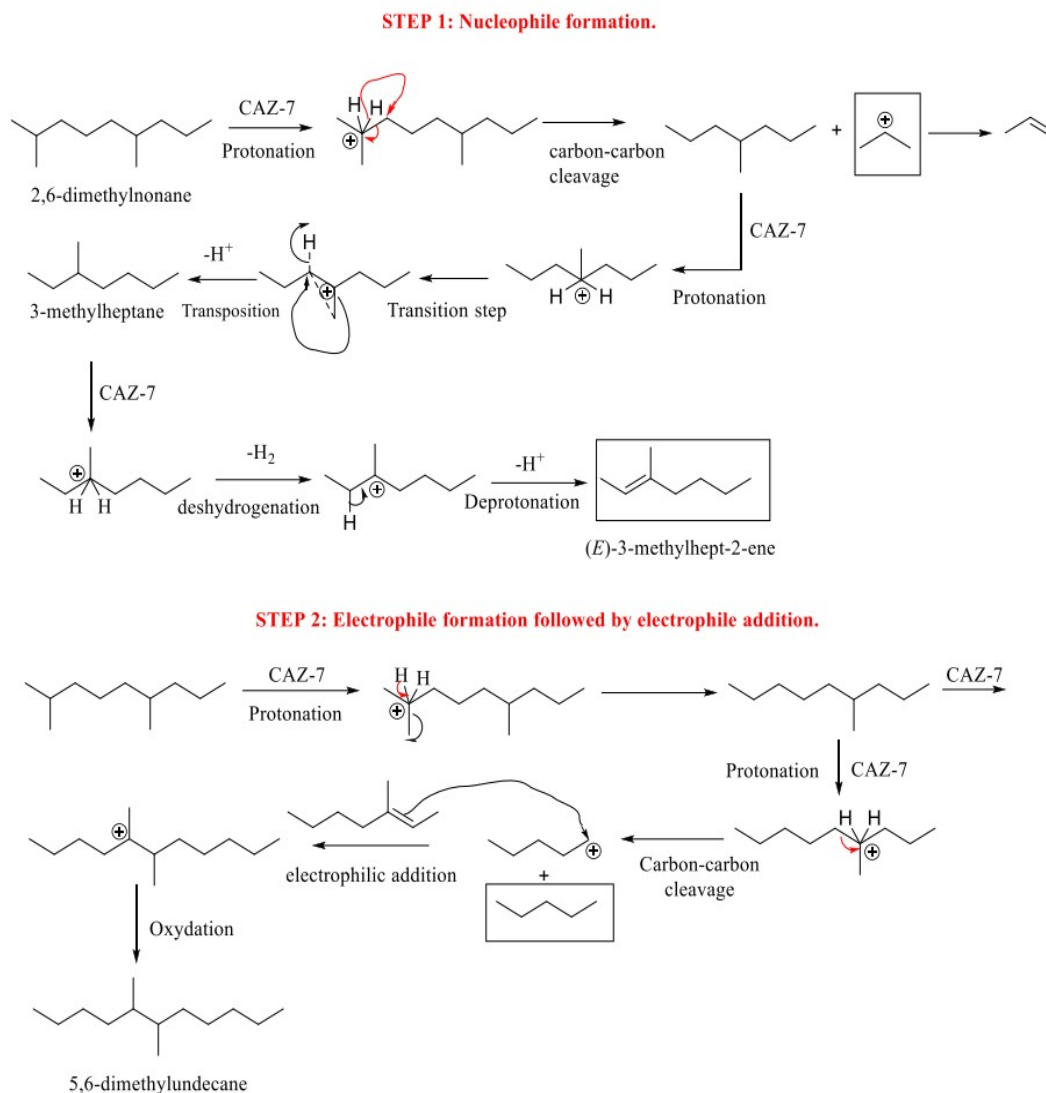


**Fig. 13. A proposal for a reaction mechanism to obtain 5,6-dimethylundecane and 3-methylheptane from 2,6-dimethylnonane, using CAZ-7 as a catalyst.**

These three reaction mechanisms show that CAZ-1, CAZ-2, and CAZ-7 favored the production of alkanes and cycloalkanes. This leads us to conclude that these synthesized zeolite catalysts are likely to be Y zeolite type zeolite catalysts. This was also corroborated by Pigot (Pigot, s. d.), who reported that these types of zeolite favor the production of n-alkanes, isoparaffins, and even cycloalkanes rather than alkenes. According to Krijn P. J et al., 2010 (de Jong et al., 2010) this particular selectivity can be explained by mesoporosity. Indeed, a Y zeolite containing mainly mesopores and a few micropores produces medium cuts ranging from C11 to C15. The results of the GC-MS analysis of the catalytic cracking products of naphtha on CAZ-1, 2 and 7 confirm those of the BET analysis (Table 6). CAZ-7, which has more mesopores than CAZ-1 and 2, favored the production of 5,6-dimethylundecane, a molecule containing thirteen carbon atoms.

### Conclusion:-

X-ray diffraction (XRD) analyses of the three zeolite catalysts (CAZ-1, CAZ-2, and CAZ-7) show a disappearance of the kaolinite, illite, and smectite peaks. This gives way to significant quartz ( $\text{SiO}_2$ ) peaks, reflecting the incorporation of silica-rich sand ( $S_M$ ) used in synthesizing these zeolite catalysts. Additionally, the diffractograms of the three catalysts exhibit intense, well-resolved peaks that resemble those of highly crystalline Y zeolite standards. X-ray fluorescence (XRF) analysis yielded  $\text{SiO}_2$  and  $\text{Al}_2\text{O}_3$  content values that correspond to Silica Alumina Ratios (SAR) of 5.33 for CAZ-1, 3.27 for CAZ-2, and 3.19 for CAZ-7. The SAR of CAZ-1 belongs to the SAR range of zeolite-Y, while the SARs of CAZ-2 and CAZ-7 belong to the SAR range of intermediate Y zeolite. FT-IR analysis of CAZ-1, 2, and 7 shows characteristic bands of symmetric and asymmetric T-O-T (T = Si or Al) bond vibrations of  $\text{SiO}_4$  and  $\text{AlO}_4$  tetrahedra characteristic of zeolite structures. Peaks corresponding to aluminosilicate vibrations and to the stretching of the external asymmetry of the Si-O-Si bond were observed in the IR spectra of the synthesized zeolite catalysts. Peaks were also observed that are attributed to the external stretching of the silica framework and the conversion of the octahedral coordination of kaolinite ( $\text{Al}^{3+}$ ) to the tetrahedral coordination of metakaolinite. BET analysis of CAZ-2 and CAZ-7 shows an increase in specific surface area ( $S_{\text{BET}}$ ), micropores ( $S_{\text{micro}}$ ), and mesopores ( $S_{\text{meso}}$ ). This reflects an increase in micro- and mesoporousness during the synthesis of CAZ-2 and CAZ-7.

In contrast, a decrease in BET specific surface area was observed during the synthesis of CAZ-1. A comparable trend to that of the specific surface areas of the synthesized catalysts was observed for pore diameters ( $D_{\text{meso}}$  and  $D_{\text{micro}}$ ) and pore volumes ( $V_{\text{meso}}$  and  $V_{\text{micro}}$ ). Nitrogen ( $\text{N}_2$ ) desorption reveals a mixture of micro- and mesopores in the three uniformly distributed catalyst samples. Scanning Electron Microscopy (SEM) analysis of the three samples reveals the presence of tetrahedra ( $\text{TO}_4$ ) and hexagonal prisms, which are characteristic of zeolite catalyst morphology. This morphology contributes to the formation of  $\alpha$ -cavities (supercages) and  $\beta$ -cavities (sodalites), which are characteristic of Y zeolite. The study of the thermochemical behavior of the synthesized catalysts made it possible, first, to determine initial peaks at around  $100^\circ\text{C}$  for all three (3) catalysts. This can be explained by the elimination of water from the surface of the catalysts. At these temperatures, the mass loss is approximately 3.47% for CAZ-1, approximately 2.53% for CAZ-2, and approximately 9.24% for CAZ-7. Next are the second peaks, which are visible at approximately  $400^\circ\text{C}$  for CAZ-1,  $380^\circ\text{C}$  for CAZ-2, and  $480^\circ\text{C}$  for CAZ-7. These peaks are due to the dihydroxylation reaction of clay minerals. The mass loss value at these temperatures is almost zero for CAZ-2 and CAZ-7. However, the mass loss value for CAZ-1 at  $400^\circ\text{C}$  is 4.61%. The third peaks correspond to the structural reorganization of the synthesized zeolite catalysts, with values of  $700^\circ\text{C}$  for CAZ-1 and CAZ-2 and  $650^\circ\text{C}$  for CAZ-7. The associated mass loss values are 3.16%, 1.37%, and 2.31%, respectively. The synthesized zeolite catalysts CAZ-1, CAZ-2, and CAZ-7 exhibit similar mineralogical, chemical, physical, morphological, and thermal characteristics to Y zeolite (Y FAU) catalysts. The latter promotes the selectivity of n-alkanes, isoparaffins, and cycloalkanes over alkenes.

### References:-

1. Abdoulaye Dan Makaou, O., Gueu, S., Gourouza, M., & Yao, K. B. (2021). Development of semi-synthetic catalyst based on clay and their use in catalytic cracking of petroleum residue. *Applied Petrochemical Research*, 11(2), 147-154. <https://doi.org/10.1007/s13203-021-00268-w>
2. Abdourahmane, A. I., Gueu, S., Salam, M. A., Kone, H., & Yao, K. B. (2022). Comparative study of physico-chemical, mineralogical and morphological characteristics of clay from Niger-Maradi : Application to the synthesis of ZSM-5 aluminosilicate catalysts. 14.
3. Armor, J. N. (2011). A history of industrial catalysis. *Catalysis Today*, 163(1), 3-9. <https://doi.org/10.1016/j.cattod.2009.11.019>
4. Asghari, A., Khorrani, M. K., & Kazemi, S. H. (2019). Hierarchical H-ZSM5 zeolites based on natural kaolinite as a high-performance catalyst for methanol to aromatic hydrocarbons conversion. *Scientific Reports*, 9(1), 17526. <https://doi.org/10.1038/s41598-019-54089-y>
5. Biliget, T., Wang, Y., Nishitoba, T., Otomo, R., Park, S., Mochizuki, H., Kondo, J. N., Tatsumi, T., & Yokoi, T. (2017). Al distribution and catalytic performance of ZSM-5 zeolites synthesized with various alcohols. *Journal of Catalysis*, 353, 1-10. <https://doi.org/10.1016/j.jcat.2017.06.026>
6. Bouna, L., Ait El Fakir, A., Benlhachemi, A., Draoui, K., Ezahri, M., Bakiz, B., Villain, S., Guinneton, F., & Elalem, N. (2020). Synthesis and characterization of mesoporous geopolymer based on Moroccan kaolinite rich clay. *Applied Clay Science*, 196, 105764. <https://doi.org/10.1016/j.clay.2020.105764>
7. Breck, D. W. (1973). *Zeolite molecular sieves : Structure, chemistry, and use*.

8. Chester, A. W. (1984). Dehydrocyclization of n-hexane by highly dispersed platinum in zeolite Y. *Journal of Catalysis*, 86(1), 16-23. [https://doi.org/10.1016/0021-9517\(84\)90343-9](https://doi.org/10.1016/0021-9517(84)90343-9)
9. Chester, A. W., & Derouane, E. G. (Éds.). (2009). *Zeolite Chemistry and Catalysis*. Springer Netherlands. <https://doi.org/10.1007/978-1-4020-9678-5>
10. Contescu, A., Contescu, C., Putyera, K., & Schwarz, J. A. (1997). Surface acidity of carbons characterized by their continuous pK distribution and Boehm titration. *Carbon*, 35(1), 83-94. [https://doi.org/10.1016/S0008-6223\(96\)00125-X](https://doi.org/10.1016/S0008-6223(96)00125-X)
11. Costa, I. C. M. (2019). *Adsorption/diffusion interplay in hierarchical zeolites : Understanding the role of external surface and additional porosity* [Phdthesis]. Université de Lyon.
12. Degnan, T. F., Chitnis, G. K., & Schipper, P. H. (2000). History of ZSM-5 fluid catalytic cracking additive development at Mobil. *Microporous and Mesoporous Materials*, 35-36, 245-252. [https://doi.org/10.1016/S1387-1811\(99\)00225-5](https://doi.org/10.1016/S1387-1811(99)00225-5)
13. de Jong, K. P., Zečević, J., Friedrich, H., de Jongh, P. E., Bulut, M., van Donk, S., Kenmogne, R., Finiels, A., Hulea, V., & Fajula, F. (2010). Zeolite Y Crystals with Trimodal Porosity as Ideal Hydrocracking Catalysts. *Angewandte Chemie International Edition*, 49(52), 10074-10078. <https://doi.org/10.1002/anie.201004360>
14. Department of Chemistry and Chemical Engineering, Hunan Institute of Science and Technology, Yueyang 414 006, Hunan, P.R. China, He, L.-J., Zheng, S.-Q., Department of Chemistry and Chemical Engineering, Hunan Institute of Science and Technology, Yueyang 414 006, Hunan, P.R. China, Dai, Y.-L., & Yueyang Science and Technology Association, Yueyang 414 000, Hunan, P.R. China. (2017). An FCC Catalyst for Maximizing Gasoline Yield. *Kemija u Industriji*, 66(1-2), 9-15. <https://doi.org/10.15255/KUI.2016.028>
15. Emam, E. A. (2013). *Clays as Catalysts in Petroleum Refining Industry*. 3(4), 20.
16. Enterría, M., Suárez-García, F., Martínez-Alonso, A., & Tascón, J. M. D. (2014). Preparation of hierarchical micro-mesoporous aluminosilicate composites by simple Y zeolite/MCM-48 silica assembly. *Journal of Alloys and Compounds*, 583, 60-69. <https://doi.org/10.1016/j.jallcom.2013.08.137>
17. Ghrib, Y., Frini-Srasra, N., & Srasra, E. (2017). Synthesis of ZSM-5 zeolite from metakaolinite : Effects of the SiO<sub>2</sub>/Al<sub>2</sub>O<sub>3</sub> molar ratio, the initial precursor and the presence of organic template agent. *Surface Engineering and Applied Electrochemistry*, 53(1), 64-70. <https://doi.org/10.3103/S1068375517010057>
18. Gonçalves, M. L., Dimitrov, L. D., Jordão, M. H., Wallau, M., & Urquieta-González, E. A. (2008). Synthesis of mesoporous ZSM-5 by crystallisation of aged gels in the presence of cetyltrimethylammonium cations. *Catalysis Today*, 133-135, 69.
19. Goupy, J., & Creighton, L. (2006). *Introduction aux plans d'expériences* (3e éd). Dunod « L'Usine nouvelle ».
20. Hussain, A. I., Aitani, A. M., Kubû, M., Čejka, J., & Al-Khattaf, S. (2016). Catalytic cracking of Arabian Light VGO over novel zeolites as FCC catalyst additives for maximizing propylene yield. *Fuel*, 167, 226-239. <https://doi.org/10.1016/j.fuel.2015.11.065>
21. Ibarra, Á., Hita, I., Azkoiti, M. J., Arandes, J. M., & Bilbao, J. (2019). Catalytic cracking of raw bio-oil under FCC unit conditions over different zeolite-based catalysts. *Journal of Industrial and Engineering Chemistry*, 78, 372-382. <https://doi.org/10.1016/j.jiec.2019.05.032>
22. Jia, H., Du, T., Fang, X., Gong, H., Qiu, Z., Li, Y., & Wang, Y. (2021). Synthesis of Template-Free ZSM-5 from Rice Husk Ash at Low Temperatures and Its CO<sub>2</sub> Adsorption Performance. *ACS Omega*, 6(5), 3961-3972. <https://doi.org/10.1021/acsomega.0c05842>
23. Kaban, I. (s. d.). *Synthèse des matériaux nanoporeux pour la décontamination moléculaire et le stockage d'énergie*.
24. Khoshbin, R., & Karimzadeh, R. (2017). Synthesis of mesoporous ZSM-5 from rice husk ash with ultrasound assisted alkali-treatment method used in catalytic cracking of light naphtha. *Advanced Powder Technology*, 28(8), 1888-1897. <https://doi.org/10.1016/j.appt.2017.04.024>
25. Kovo, A. S., Hernandez, O., & Holmes, S. M. (2009). Synthesis and characterization of zeolite Y and ZSM-5 from Nigerian Ahoko Kaolin using a novel, lower temperature, metakaolinization technique. *Journal of Materials Chemistry*, 19(34), 6207. <https://doi.org/10.1039/b907554b>
26. Li, X.-Y., Jiang, Y., Liu, X.-Q., Shi, L.-Y., Zhang, D.-Y., & Sun, L.-B. (2017). Direct Synthesis of Zeolites from a Natural Clay, Attapulgit. *ACS Sustainable Chemistry & Engineering*, 5(7), 6124-6130. <https://doi.org/10.1021/acssuschemeng.7b01001>
27. Liu, Y., Han, S., Guan, D., Chen, S., Wu, Y., Yang, Y., & Jiang, N. (2019). Rapid green synthesis of ZSM-5 zeolite from leached illite clay. *Microporous and Mesoporous Materials*, 280, 324-330. <https://doi.org/10.1016/j.micromeso.2019.02.027>
28. Margeta, K., & Farkaš, A. (2020). Introductory Chapter : Zeolites - From Discovery to New Applications on the Global Market. In K. Margeta & A. Farkaš (Éds.), *Zeolites—New Challenges* (p. 10). IntechOpen. <https://doi.org/10.5772/intechopen.92907>

29. Murat, M., & Bachiorrini, A. (1982). Corrélation entre l'état d'amorphisation et l'hydraulicité du métakaolin. *Bulletin de Minéralogie*, 105(5), 543-555. <https://doi.org/10.3406/bulmi.1982.7577>
30. Otmani, S. (2006). *Valorisation des charges lourdes compoundées par le craquage catalytique*. 88.
31. P. Leprince. (s. d.). *Le raffinage du pétrole—Tome 3, Collectif Technip—Librairie Eyrolles*.
32. Pan, F., Lu, X., Wang, T., & Yan, Y. (2017). Submicron ZSM-5 synthesized by green and fast route. *Materials Letters*, 196, 245-247. <https://doi.org/10.1016/j.matlet.2017.03.060>
33. Percival, H. J., Duncan, J. F., & Foster, P. K. (1974a). Interpretation of the Kaolinite-Mullite Reaction Sequence from Infrared Absorption Spectra. *Journal of the American Ceramic Society*, 57(2), 57-61. <https://doi.org/10.1111/j.1151-2916.1974.tb10813.x>
34. Percival, H. J., Duncan, J. F., & Foster, P. K. (1974b). Interpretation of the Kaolinite-Mullite Reaction Sequence from Infrared Absorption Spectra. *Journal of the American Ceramic Society*, 57(2), 57-61. <https://doi.org/10.1111/j.1151-2916.1974.tb10813.x>
35. Pigot, J.-B. (s. d.). *Dynamique multi-échelle et échange inter-porosité par relaxométrie RMN au sein de zéolithes mésoporisées*.
36. *Plans d'expérience : Constructions et analyses statistiques* (Vol. 67). (2010). Springer Berlin Heidelberg. <https://doi.org/10.1007/978-3-642-11472-4>
37. Qin, Z., Shen, B., Gao, X., Lin, F., Wang, B., & Xu, C. (2011). Mesoporous Y zeolite with homogeneous aluminum distribution obtained by sequential desilication–dealumination and its performance in the catalytic cracking of cumene and 1,3,5-triisopropylbenzene. *Journal of Catalysis*, 278, 266-275. <https://doi.org/10.1016/j.jcat.2010.12.013>
38. Qoniah, I., Prasetyoko, D., Bahruji, H., Triwahyono, S., Jalil, A. A., Suprpto, Hartati, & Purbaningias, T. E. (2015). Direct synthesis of mesoporous aluminosilicates from Indonesian kaolin clay without calcination. *Applied Clay Science*, 118, 290-294. <https://doi.org/10.1016/j.clay.2015.10.007>
39. Rabo, J. A., & Gajda, G. J. (1990). Acid Function in Zeolites : Recent Progress. In D. Barthomeuf, E. G. Derouane, & W. Hölderich (Éds.), *Guidelines for Mastering the Properties of Molecular Sieves* (Vol. 221, p. 273-297). Springer US. [https://doi.org/10.1007/978-1-4684-5787-2\\_17](https://doi.org/10.1007/978-1-4684-5787-2_17)
40. Ribeiro, A. M., Machado Júnior, H. F., & Costa, D. A. (2013). Kaolin and commercial fcc catalysts in the cracking of loads of polypropylene under refinery conditions. *Brazilian Journal of Chemical Engineering*, 30(4), 825-834. <https://doi.org/10.1590/S0104-66322013000400014>
41. Trambouze, P. (1999). *Raffinage du pétrole Tome 4—Matériels et équipements*. Editions TECHNIP.
42. Traore, K. (2003). *Frittage à basse température d'une argile kaolinique du Burkina Faso : Transformations thermiques et réorganisations structurales = Low temperature sintering of a kaolinitic clay from Burkina Faso : Thermal transformations and structural reorganizations*. Limoges.
43. Wu, M., Jiang, W., Jiang, J., Zou, Y., Zhang, P., Mao, P., Xu, Y., & Shi, Y. (2020). Synthesis of ZSM-5 zeolites using palygorskite as raw material under solvent-free conditions. *Bulletin of Materials Science*, 43(1), 289. <https://doi.org/10.1007/s12034-020-02263-8>
44. Yang, S., Yuan, P., He, H., Qin, Z., Zhou, Q., Zhu, J., & Liu, D. (2012). Effect of reaction temperature on grafting of  $\gamma$ -aminopropyl triethoxysilane (APTES) onto kaolinite. *Applied Clay Science*, 62-63, 8-14. <https://doi.org/10.1016/j.clay.2012.04.006>
45. Youssef, H., Ibrahim, D., & Komarneni, S. (2008). Microwave-assisted versus conventional synthesis of zeolite A from metakaolinite. *Microporous and Mesoporous Materials*, 115(3), 527-534. <https://doi.org/10.1016/j.micromeso.2008.02.030>
46. Yue, Y., Hu, Y., Dong, P., Li, X., Liu, H., Bao, J., Wang, T., Bi, X., Zhu, H., Yuan, P., Bai, Z., & Bao, X. (2020). Mesoscale depolymerization of natural rectorite mineral via a quasi-solid-phase approach for zeolite synthesis. *Chemical Engineering Science*, 220, 115635. <https://doi.org/10.1016/j.ces.2020.115635>
47. Yue, Y., Kang, Y., Bai, Y., Gu, L., Liu, H., Bao, J., Wang, T., Yuan, P., Zhu, H., Bai, Z., & Bao, X. (2018). Seed-assisted, template-free synthesis of ZSM-5 zeolite from natural aluminosilicate minerals. *Applied Clay Science*, 158, 177-185. <https://doi.org/10.1016/j.clay.2018.03.025>
48. Zhang, L., Bao, Z., Xia, S., Lu, Q., & Walters, K. (2018). Catalytic Pyrolysis of Biomass and Polymer Wastes. *Catalysts*, 8(12), 659. <https://doi.org/10.3390/catal8120659>
49. Zhang, Z., Liu, Z., Feng, R., Liu, P., & Yan, Z. (2014). The development of FCC catalysts for producing FCC gasoline with high octane numbers. *Applied Petrochemical Research*, 4(4), 379-383. <https://doi.org/10.1007/s13203-014-0075-9>
50. Zibouche, F., Boudissa, N., Irekti, A., & Abadlia, M. T. (s. d.). *Géopolymérisation d'aluminosilicates. Influence des rapports Silice/Alumine*.

51. Zibouche, F., Kerdjoudj, H., de Lacaillerie, J.-B. d'Espinose, & Van Damme, H. (2009). Geopolymers from Algerian metakaolin. Influence of secondary minerals. *Applied Clay Science*, 43(3), 453-458.  
<https://doi.org/10.1016/j.clay.2008.11.001>
52. Zimmermann, N. E. R., & Haranczyk, M. (2016). History and Utility of Zeolite Framework-Type Discovery from a Data-Science Perspective. *Crystal Growth & Design*, 16(6), 3043-3048.  
<https://doi.org/10.1021/acs.cgd.6b00272>.